Graph Inference Acceleration by Learning MLPs on Graphs without Supervision

Zehong Wang [1] **Zheyuan Zhang** [1] **Chuxu Zhang** [2] **Yanfang Ye** [1]

Abstract

Graph Neural Networks (GNNs) have demonstrated effectiveness in various graph learning tasks, yet their reliance on message-passing constraints their deployment in latency-sensitive applications such as financial fraud detection. Recent works have explored distilling knowledge from GNNs to Multi-Layer Perceptrons (MLPs) to accelerate inference. However, this task-specific supervised distillation limits generalization to unseen nodes, which are prevalent in latency-sensitive applications. To this end, we present **SIMMLP**, a **SIM**ple yet effective framework for learning **MLP**s on graphs without supervision, to enhance generalization. SIMMLP employs self-supervised alignment between GNNs and MLPs to capture the fine-grained and generalizable correlation between node features and graph structures, and proposes two strategies to alleviate the risk of trivial solutions. Theoretically, we comprehensively analyze SIMMLP to demonstrate its equivalence to GNNs in the optimal case and its generalization capability. Empirically, SIMMLP outperforms state-of-the-art baselines, especially in settings with unseen nodes. In particular, it obtains significant performance gains **(7∼26%)** over MLPs and inference acceleration over GNNs **(90∼126×)** on large-scale graph datasets. Our codes are available at: https://github.com/Zehong-Wang/SimMLP.

1. Introduction

Due to the ubiquity of graph-structured data, Graph Neural Networks (GNNs) have drawn significant attention in recent years. Generally, GNNs are based on message-passing (Gilmer et al., 2017) to learn representations of given graphs. Despite their effectiveness in various graph learning tasks, due to the computational overhead of neighborhood fetching (Zhang et al., 2022), GNNs still face limitations of the deployment in latency-sensitive applications, e.g., financial fraud detection (Wang et al., 2021). To solve this problem, existing works mainly adopt quantization (Ding et al., 2021), pruning (Zhou et al., 2021), and knowledge distillation (Yan et al., 2020) for graph inference acceleration. However, these accelerations are highly restricted, as they still need to fetch neighborhoods.

To address this issue, Multi-Layer Perceptrons (MLPs), trained solely on node features, emerge as efficient alternatives for latency-sensitive applications. Despite the considerable acceleration, they inevitably sacrifice the model performance due to the incapability of learning structural information. To enhance the performance, researchers have explored distilling knowledge from pre-trained GNN teachers into MLP students (Zhang et al., 2022; Tian et al., 2023; Wang et al., 2023; Yang et al., 2023b). In particular, these methods mimic the predictions of GNNs using MLPs, maximizing the correlation between GNNs and MLPs in the label space. Despite the progress, the task-specific supervised learning process of existing methods hinders the model generalization, especially for unseen nodes, which are common in latency-sensitive applications (Weber et al., 2019). To this end, we naturally ask: ***How to align GNNs and MLPs to obtain more generalizable node embeddings for graph inference acceleration?***

To answer the question, we bring a new insight: modeling the fine-grained correlation between node features and graph structures can improve the generalization of node embeddings (Tian et al., 2020a). Motivated by this insight, we propose to model the alignment between GNNs and MLPs in the embedding space, which preserves intricate semantic knowledge. Accordingly, we present a **SIM**ple yet effective framework for learning **MLP**s on graphs without supervision (**SIMMLP**). The framework employs self-supervised alignment to maximize the consistency between GNNs and MLPs, improving model generalization (Cabannes et al., 2023). We further propose two strategies to prevent the potential trivial solution, a common issue in self-supervised models (He et al., 2020; Grill et al., 2020). Theoretically, we demonstrate the equivalence between SIMMLP (in the optimal case) and GNNs in terms of the learning objective, even though SIMMLP is an MLP-based method. To further evaluate this, we show SIMMLP and GNNs share two key inductive biases: homophily philosophy and local structure importance. In addition, we interpret SIMMLP

[1]University of Notre Dame, Indiana, USA [2]Brandeis University, Massachusetts, USA. Correspondence to: Yanfang Ye <yye7@nd.edu>.

from the perspective of information bottleneck to demonstrate its generalization capability. Empirically, we show the effectiveness of SIMMLP over ten public benchmarks on standard transductive node classification task. Furthermore, we formulate two more realistic settings, namely, inductive and cold-start settings, to simulate the emergence of new nodes, showing the generalizability of SIMMLP on unseen nodes. In terms of inference efficiency, SIMMLP exhibits remarkable acceleration compared to GNNs **(90∼126×)** and other acceleration techniques **(5∼90×)**.

Other Benefits of SIMMLP. SIMMLP utilizes self-supervised alignment to bring three additional benefits over existing MLP learning methods with supervised knowledge distillation. Firstly, it performs better with sparse labels (Chen et al., 2020c), where label acquisition is challenging in many real latency-sensitive applications (Weber et al., 2019). Secondly, SIMMLP is robust to noisy graphs, whereas existing methods generally fall short (Guo et al., 2023). Lastly, SIMMLP acquires task-agnostic knowledge that is generalizable across diverse tasks (Sun et al., 2023). These advantages are demonstrated in the appendix.

2. Related Work

Graph Neural Networks encode node embeddings by *passing* and *aggregating* neighborhood messages. For example, GCN (Kipf & Welling, 2017) employs normalized Laplacian matrix to guide neighborhood aggregation, GraphSAGE (Hamilton et al., 2017) utilizes neighborhood sampling and various aggregation functions, and GAT (Veličković et al., 2018) applies attention mechanisms. In addition, SGC (Wu et al., 2019) and APPNP (Gasteiger et al., 2019) decompose feature transformation and message-passing for rapid inference. These methods are proven to be expressive in recent studies (Han et al., 2023; Yang et al., 2023a). Despite their success, the neighborhood dependency inevitably constrains the inference speed. We aim to mitigate this in the paper.

Self-Supervised Learning (SSL) (Chen et al., 2020b; He et al., 2020) acts as a pre-training strategy for learning discriminative (Tian et al., 2020b) and generalizable (Huang et al., 2023) representations without supervision. Numerous studies extend SSL on graphs to train GNNs (Veličković et al., 2019; Hassani & Khasahmadi, 2020; Zhu et al., 2020; 2021; Thakoor et al., 2022; Hou et al., 2022; Sun et al., 2023). In particular, GCA (Zhu et al., 2021) extends instance discrimination (Chen et al., 2020b) to align similar instances in two graph views, and BGRL (Thakoor et al., 2022) employs bootstrapping (Grill et al., 2020) to further enhance training efficiency. However, the dependency on neighborhood information still limits the inference speed.

Inference Acceleration on GNNs encompasses quantization (Gupta et al., 2015; Jacob et al., 2018), pruning (Han et al., 2015; Frankle & Carbin, 2019), and knowledge distillation (KD) (Hinton et al., 2015; Sun et al., 2019). Quantization (Ding et al., 2021) approximates continuous data with limited discrete values, pruning (Zhou et al., 2021) involves dropping redundant neurons in the model, and KD focuses on transferring knowledge from large models to small models (Yan et al., 2020). However, they still need to fetch neighborhoods, resulting in constrained inference acceleration. Considering this, GLNN (Zhang et al., 2022) utilizes structure-independent MLPs for predictions, significantly accelerating inference by eliminating message-passing. However, it distills knowledge from pre-trained GNNs into MLPs in the label space, inevitably compromising generalization on unseen nodes. Following works further integrate structural information via positional embedding (Tian et al., 2023; Wang et al., 2023), label propagation (Yang et al., 2021), or motif cookbook (Yang et al., 2023b), but they still *mimic* the predictions of GNNs, failing to learn generalizable knowledge. In parallel, GraphMLP (Hu et al., 2021) and following works (Dong et al., 2022; Liu et al., 2022) employ neighborhood-aware distillation to train MLPs, albeit limited to the transductive setting. Unlike these methods, SIMMLP aligns GNNs and MLPs in the embedding space via self-supervised learning, preserving more fine-grained and generalizable information for better performance on unseen nodes.

3. Methodology

3.1. Preliminary

Notations. Considering a graph $\mathcal{G} = (\boldsymbol{A}, \boldsymbol{X})$ consisting of node set $\mathcal{V}$ and edge set E, with N nodes in total, we have node features $\boldsymbol{X} \in \mathbb{R}^{N\times d}$ with dimension d and adjacent matrix $\boldsymbol{A} \in \{0,1\}^{|\mathcal{V}|\times|\mathcal{V}|}$, where $\boldsymbol{A}_{ij} = 1$ iff $e_{i,j} \in E$, and $\boldsymbol{A}_{ij} = 0$ otherwise. We use GNNs and MLPs to make predictions over the graph $\mathcal{G}$. GNNs follow the message-passing framework that consists of UPDATE$(\cdot)$ and AGGREGATE$(\cdot)$, iteratively updating node embeddings by neighborhood information aggregation. A GNN encoder $\phi(\cdot,\cdot)$ takes node features $\boldsymbol{x}_i$ and graph structure $\boldsymbol{A}$ as input, and output the structure-aware node embeddings $\boldsymbol{h}_i^{GNN}$. It follows a prediction head to classify nodes into different classes, defined as

$$\boldsymbol{h}_i^{GNN} = \phi(\boldsymbol{x}_i, \boldsymbol{A}), \quad \hat{\boldsymbol{y}}_i^{GNN} = \text{head}^{GNN}(\boldsymbol{h}_i^{GNN}). \quad (1)$$

The GNNs highly rely on neighborhood information, where neighborhood fetching poses considerable computational overhead during the inference. On the contrary, MLPs $\mathcal{E}(\cdot)$ take the node feature $\boldsymbol{x}_i$ as input and output the node embeddings $\boldsymbol{h}_i^{MLP}$, achieving fast inference by alleviating the neighborhood-fetching. The embeddings are then decoded via a prediction head:

$$\boldsymbol{h}_i^{MLP} = \mathcal{E}(\boldsymbol{x}_i), \quad \hat{\boldsymbol{y}}_i^{MLP} = \text{head}^{MLP}(\boldsymbol{h}_i^{MLP}). \quad (2)$$

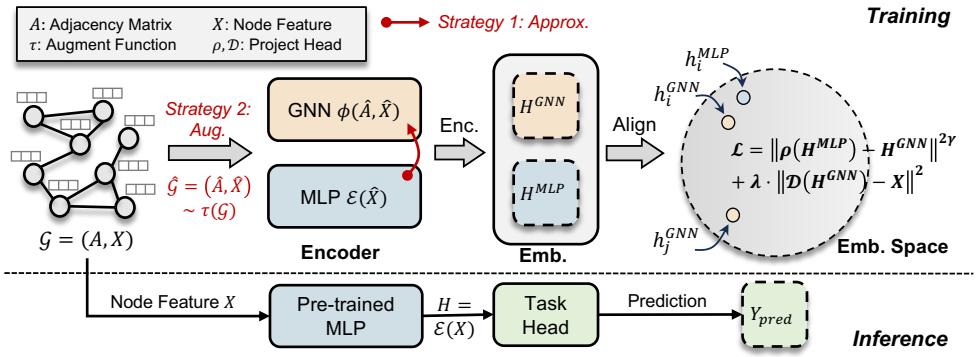

Figure 1. Overview of the SIMMLP framework. In training, SIMMLP separately leverages GNN and MLP encoders to obtain node embeddings, and then employs a self-supervised alignment loss to maximize their consistency in the embedding space. To prevent the risk of trivial solutions, SIMMLP further applies two strategies discussed in Section 3.3. In inference, SIMMLP only utilizes the pre-trained MLP to encode node embeddings, achieving substantial acceleration by eliminating the need for neighborhood fetching.

Although MLPs provide significantly faster inference over graph-structured datasets, the omitting of structural information inevitably sacrifices the model performance.

Training MLPs on Graphs. To leverage the structural learning capability of GNNs and the fast inference of MLPs, researchers propose methods to train MLPs on graphs. A prevalent method is to distill knowledge from pre-trained GNN teachers to MLP students by mimicking the predictions of GNNs (Zhang et al., 2022). During the inference, only the MLP is leveraged to encode node embeddings and make predictions, leading to a substantial inference acceleration. The objective function is defined as

$$\mathcal{L} = \sum_{i \in \mathcal{V}_{train}} \mathcal{L}_{CE}(\hat{\boldsymbol{y}}_i^{MLP}, \boldsymbol{y}_i) + \lambda \sum_{i \in \mathcal{V}} \mathcal{L}_{KD}(\hat{\boldsymbol{y}}_i^{MLP}, \hat{\boldsymbol{y}}_i^{GNN}), \tag{3}$$

where $\mathcal{L}_{CE}$ is the cross-entropy between the prediction and ground-truth, and $\mathcal{L}_{KD}$ optimizes the KL-divergence between predictions of teacher GNN and student MLP. Despite the significant inference acceleration, the alignment in the label space maximizes the task-specific correlation between GNNs and MLPs, failing to capture the fine-grained and generalizable relationship between node features and graph structures (Tian et al., 2020a). This limits the generalization on unseen nodes. To this end, SIMMLP applies self-supervised learning to align GNNs and MLPs in a more intricate embedding space, enhancing model generalization.

3.2. Framework

We present **SIMMLP**: a **SIM**ple yet effective framework for learning **MLP**s on graphs without supervision. The framework consists of three components: (1) *GNN encoder*, (2) *MLP encoder*, and (3) *alignment loss*. The choice of GNN encoder is arbitrary; we adopt the commonly used GCN (Kipf & Welling, 2017) for simplicity. As illustrated in Figure 1, SIMMLP maximizes the consistency between GNN and MLP via self-supervised alignment loss. Specifically, given a graph $\mathcal{G} = (\boldsymbol{A}, \boldsymbol{X})$, we use GNN encoder $\phi(\cdot,\cdot)$ to extract structure-aware GNN embeddings $\boldsymbol{h}_i^{GNN}$ and MLP encoder $\mathcal{E}(\cdot)$ to obtain structure-free MLP embeddings $\boldsymbol{h}_i^{MLP}$. For alignment, we employ the loss function

$$\mathcal{L} = \sum_{i \in \mathcal{V}} \underbrace{\|\rho(\boldsymbol{h}_i^{MLP}) - \boldsymbol{h}_i^{GNN}\|^{2\gamma}}_{invariance} + \lambda \underbrace{\|\mathcal{D}(\boldsymbol{h}_i^{GNN}) - \boldsymbol{x}_i\|^2}_{reconstruction}, \tag{4}$$

where $\gamma \geq 1$ serves as a scaling term, akin to an adaptive sample reweighing technique (Lin et al., 2017), and λ denotes the trade-off coefficient. The projector $\rho(\cdot), \mathcal{D}(\cdot)$ can either be identity or learnable; we opt for a non-linear MLP to enhance the expressiveness in estimating instance distances (Chen et al., 2020b). The invariance term ensures the alignment between GNN and MLP embeddings (Grill et al., 2020), modeling the fine-grained and generalizable correlation between node features and localized graph structures. The reconstruction term acts as a regularizer to prevent the potential distribution shift (Batson & Royer, 2019), providing better signals for training MLPs. Following, we reformulate Equation 4 to show the optimal MLP encoder.

Proposition 3.1. *Suppose $\mathcal{G} = (\boldsymbol{A}, \boldsymbol{X})$ is sampled from a latent graph $\mathcal{G}_\mathcal{I} = (\boldsymbol{A}, \boldsymbol{F})$, $\mathcal{G} \sim P(\mathcal{G}_\mathcal{I})$, and $\boldsymbol{F}^*$ is the lossless compression of $\boldsymbol{F}$ that $\mathbb{E}[\boldsymbol{X}|\boldsymbol{A}, \boldsymbol{F}^*] = \boldsymbol{F}$. Let ρ be an identity projector, and $\lambda = 1, \gamma = 1$. The optimal MLP encoder $\mathcal{E}^*$ satisfies*

$$\begin{aligned} \mathcal{E}^* = \arg\min_{\mathcal{E}} \mathbb{E}\left[\left\|\boldsymbol{H}^{MLP} - \boldsymbol{F}^*\right\|^2 + \left\|\boldsymbol{H}^{GNN} - \boldsymbol{F}^*\right\|^2\right] \\ + \mathbb{E}\left[\left\|\mathcal{D}(\boldsymbol{H}^{GNN}) - \boldsymbol{X}\right\|^2\right] \\ - 2\mathbb{E}_{\boldsymbol{F}^*}\left[\sum_i \mathrm{Cov}(\boldsymbol{H}_i^{MLP}, \boldsymbol{H}_i^{GNN}) | \boldsymbol{F}^*\right]. \end{aligned} \tag{5}$$

The proof is in Appendix A.1. That is, the alignment loss implicitly enables the learned embeddings invariant to latent variables (Muthén, 2004; Xie et al., 2022), and maximizes the consistency between GNNs and MLPs in covariance.

Risk. Unlike distilling knowledge from pre-trained GNNs

to MLPs in the label space (Zhang et al., 2022), alignment in the embedding space via self-supervised loss is prone to trivial solutions (Jing et al., 2022). Following we discuss some design choices to prevent this issue.

3.3. Preventing Trivial Solutions

SIMMLP is based on the principle that similar instances are predictive to each other (Grill et al., 2020; Zbontar et al., 2021). However, directly minimizing the node embedding distance (Equation 4) is prone to trivial solutions. For example, if encoders yield constant embeddings for each node, this would trivially minimize the distance through non-discriminative embeddings, leading to low training loss but also poor model accuracy. We hypothesize the inconsistency between encoders (He et al., 2020) and the lack of data diversity (Tian et al., 2020b) are two causes of trivial solutions. Encoder inconsistency may result in the same node being projected in different embedding spaces, leading to unreliable similarity measurements. This would lead to an unreliable optimization process, which may learn simplistic and non-informative embeddings (Jing et al., 2022). The lack of data diversity may lead the model to converge on simple patterns, e.g., output the original node features[1]. However, if a single instance can be represented through multi-views, the encoders would not simply learn a constant mapping for all instances; they must identify the latent patterns of multiple views. Considering these challenges, we present two strategies to prevent these two causes of the trivial solution, respectively.

Strategy 1: Enhancing Consistency between GNN and MLP via Approximation

The consistency between encoders is highly sensitive to model optimization (He et al., 2020). As evidenced in Figure 2, randomly optimizing two encoders (w/o Approx.) may fail to preserve their consistency, thus leading to trivial solutions (indicated by low loss and accuracy). To preserve the consistency, existing works utilize moving average to update the encoder parameters $\theta_1 \leftarrow m\theta_1 + (1-m)\theta_2$[2] (He et al., 2020; Grill et al., 2020). This enables the encoders to project instances into similar embedding spaces.

For SIMMLP with different encoder architectures, it is challenging to enhance their consistency using existing techniques. To this end, we propose a simple method to *approximate* GNNs using MLPs, in order to maintain the correlation between GNN and MLP embeddings. Specifically, we employ MLPs to encode node embeddings and subsequently conduct message-passing, simulating the GNN learning process. The message-passing rule is arbitrary (Gilmer et al., 2017); we take 1-layer GCN as an example:

$$\text{GCN: } \boldsymbol{h}_i^G = \sigma\left(\boldsymbol{\Theta}\boldsymbol{x}_i + \textstyle\sum_{(i,j)\in E} \alpha_{ij}\boldsymbol{\Theta}\boldsymbol{x}_j\right), \quad (6)$$

$$\text{Approx.: } \boldsymbol{h}_i^G = \sigma\left(\boldsymbol{h}_i^M + \textstyle\sum_{(i,j)\in E} \alpha_{ij}\,\boldsymbol{h}_j^M\right), \quad (7)$$

where $\boldsymbol{h}^M$, $\boldsymbol{h}^G$ are abbreviations of $\boldsymbol{h}^{MLP}$ and $\boldsymbol{h}^{GNN}$, $\boldsymbol{\Theta}$ is the learnable weight matrix, α_{ij} denotes the GCN aggregation weight (Kipf & Welling, 2017), and $\sigma(\cdot)$ is the activation. The form of our approximation is similar to SGC (Wu et al., 2019) and APPNP (Gasteiger et al., 2019), which decompose feature transformation and message-passing to reduce model complexity and redundant computations. Unlikely, SIMMLP applies the strategy to enhance the consistency between GNN and MLP encoders. As shown in Figure 2, applying the approximation strategy can significantly mitigate the risk of model collapse.

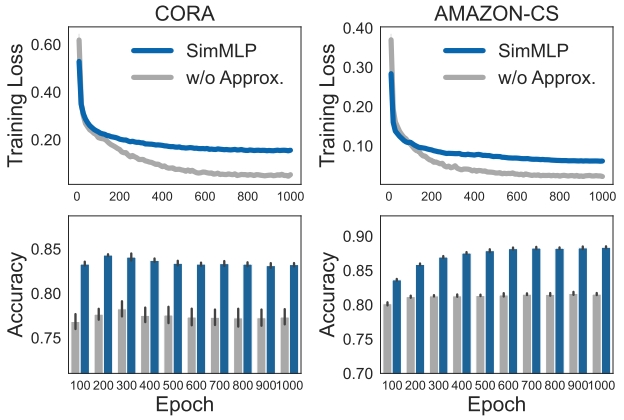

Figure 2. The training curve and model accuracy with and without Strategy 1 (Approx.). When the GNN and MLP encoders are randomly optimized (w/o Approx.), the model collapse happens. See Appendix E.2 for more results.

Strategy 2: Enhancing Data Diversity via Augmentation

Table 1. Model performance with and without Strategy 2 (Aug.). More analysis is in Appendix E.4.

Methods	Cora	Citeseer	Computer	Co-CS	Co-Phys
SIMMLP	**84.6**$_{\pm 0.2}$	**73.5**$_{\pm 0.5}$	**88.5**$_{\pm 0.2}$	**94.9**$_{\pm 0.1}$	**96.2**$_{\pm 0.0}$
w/o Aug.	82.1$_{\pm 0.5}$	71.8$_{\pm 0.4}$	87.1$_{\pm 0.2}$	93.1$_{\pm 0.1}$	94.6$_{\pm 0.1}$

Enhancing the diversity of the same instance (Lee et al., 2020) is another approach to prevent the trivial solution. We use augmentation techniques (You et al., 2020; Zhao et al., 2021) to produce multi-views of nodes, enabling a single node to have multiple and various embeddings. We define the augmentation as

$$\hat{\mathcal{G}} = (\hat{\boldsymbol{A}}, \hat{\boldsymbol{X}}) \sim t(\mathcal{G}), s.t., t(\mathcal{G}) = \langle q_e(\boldsymbol{A}), q_f(\boldsymbol{X})\rangle, \quad (8)$$

[1]Considering 1-layer GCN (Kipf & Welling, 2017) and 1-layer MLP, the output of GCN is $\boldsymbol{H}_1 = \hat{\boldsymbol{A}}\boldsymbol{W}_1\boldsymbol{X}$ where $\hat{\boldsymbol{A}} = \tilde{\boldsymbol{D}}^{-1/2}\tilde{\boldsymbol{A}}\tilde{\boldsymbol{D}}^{-1/2}$, $\tilde{\boldsymbol{A}} = \boldsymbol{A} + \boldsymbol{I}$ and $\tilde{\boldsymbol{D}}$ is the diagonal matrix of node degree of $\tilde{\boldsymbol{A}}$, and the output of MLP is $\boldsymbol{H}_2 = \boldsymbol{W}_2\boldsymbol{X}$. The trivial solution can be met by learning $\hat{\boldsymbol{A}}\boldsymbol{W}_1 = \boldsymbol{I}$ and $\boldsymbol{W}_2 = \boldsymbol{I}$, that is $\boldsymbol{H}_1 = \boldsymbol{H}_2 = \boldsymbol{X}$. In cases $\hat{\boldsymbol{A}}$ is non-invertible, finding an approximation where $\hat{\boldsymbol{A}}\boldsymbol{W}_1 \approx \boldsymbol{I}$ is relatively straightforward.

[2]$m \in [0, 1)$ is the momentum coefficient and $\theta_{1,2}$ indicates the parameters of two encoders. Here θ_2 is optimized by the back-propagation and θ_1 is updated by θ_2

where $t(\cdot)$ is the augmentation function consisting of structural augmentation $q_e(\cdot)$ and node feature augmentation $q_f(\cdot)$. For simplicity, we use random edge masking and node feature masking with pre-defined augmentation ratios (Zhu et al., 2020). The augmentation generates additional node-subgraph pairs to facilitate the model training (Xu et al., 2021)[3]. The benefit is presented in Table 1.

Alternative Strategies. To prevent trivial solutions, Grill et al. (2020) uses stop-gradient to construct asymmetric update, Caron et al. (2018; 2020) apply prototype learning to leverage semantic knowledge, Zbontar et al. (2021) minimizes the redundency between two encoders, and Chen et al. (2020b) introduces negative samples to push dissimilar nodes apart. We leave these in the future work.

4. Theoretical Analysis

4.1. Mutual Information Maximization

Table 2. The learning objective from the perspective of mutual information maximization. Our SIMMLP is equivalent to GNNs in the optimal case, while other MLP-based methods lack the capability of (fully) incorporating structural information.

	Methods	Learning Objective
	GNNs (Kipf & Welling, 2017; Hamilton et al., 2017)	$\sum_{i\in\mathcal{V}} I(\boldsymbol{y}_i;\mathcal{S}_i) = \sum_{i\in\mathcal{V}} I(\boldsymbol{y}_i;\boldsymbol{X}^{[i]}) + \sum_{i\in\mathcal{V}} I(\boldsymbol{y}_i;\boldsymbol{A}^{[i]}\|\boldsymbol{X}^{[i]})$
MLP	MLP (Zhang et al., 2022)	$\sum_{i\in\mathcal{V}} I(\boldsymbol{x}_i;\boldsymbol{y}_i)$
MLP	GLNN (Zhang et al., 2022)	$\sum_{i\in\mathcal{V}} I(\boldsymbol{x}_i;\boldsymbol{y}_i\|\mathcal{S}_i) + I(\boldsymbol{x}_i;\boldsymbol{y}_i)$
MLP	NOSMOG (Tian et al., 2023) GENN (Wang et al., 2023)	$\sum_{i\in\mathcal{V}} I(\boldsymbol{x}_i;\boldsymbol{y}_i\|\mathcal{S}_i) + I(\boldsymbol{x}_i;\boldsymbol{y}_i) + I(\boldsymbol{A};\boldsymbol{y}_i)$
MLP	**SIMMLP (Ours)**	$\sum_{i\in\mathcal{V}} I(\boldsymbol{y}_i;\boldsymbol{x}_i) + I(\boldsymbol{x}_i;\mathcal{S}_i)$

Mutual information $I(\cdot;\cdot)$ is a concept in information theory, measuring the mutual dependency between two random variables. This has been widely used in signal processing and machine learning (Belghazi et al., 2018). Intuitively, maximizing the mutual information between two variables can increase their correlation (i.e., decrease their uncertainty). In this section, we interpret SIMMLP and existing graph learning methods from the perspective of mutual information maximization to analyze their learning objectives, as summarized in Table 2.

Firstly, we unify the notations and introduce the key lemmas. A graph $\mathcal{G} = (\boldsymbol{X}, \boldsymbol{A}, \boldsymbol{Y})$ consists of node features $\boldsymbol{X}$, graph structure $\boldsymbol{A}$ and node labels $\boldsymbol{Y}$. We define ego-graph around node i as $\mathcal{S}_i = (\boldsymbol{X}^{[i]}, \boldsymbol{A}^{[i]})$, where $\boldsymbol{X}^{[i]}$, $\boldsymbol{A}^{[i]}$ denote node features and graph structure of $\mathcal{S}_i$, respectively.

Lemma 4.1. *Minimizing the cross-entropy $H(\boldsymbol{Y};\hat{\boldsymbol{Y}}|\boldsymbol{X})$ is equivalent to maximizing the mutual information $I(\boldsymbol{X};\boldsymbol{Y})$.*

The proof is in Appendix A.2. The vanilla MLP minimizes the cross-entropy between ground-truth $\boldsymbol{Y}$ and the predictions relying on node features, i.e., $\hat{\boldsymbol{Y}}|\boldsymbol{X}$, which is equivalent to maximize the mutual information $\sum_{i\in\mathcal{V}} I(\boldsymbol{y}_i;\boldsymbol{x}_i)$. GNNs apply message-passing to leverage structural information (ego-graph) in making predictions, which aims to maximize $\sum_{i\in\mathcal{V}} I(\boldsymbol{y}_i;\mathcal{S}_i) = \sum_{i\in\mathcal{V}} I(\boldsymbol{y}_i;\boldsymbol{X}^{[i]}) + \sum_{i\in\mathcal{V}} I(\boldsymbol{y}_i;\boldsymbol{A}^{[i]}|\boldsymbol{X}^{[i]})$. GLNN distills knowledge from GNNs to MLPs, focusing on maximizing $\sum_{i\in\mathcal{V}} I(\boldsymbol{x}_i;\boldsymbol{y}_i|\mathcal{S}_i) + I(\boldsymbol{x}_i;\boldsymbol{y}_i)$, where $\boldsymbol{y}_i|\mathcal{S}_i$ denotes the soft label from GNN teachers. However, GLNN cannot explicitly utilize structural information in making predictions. Following works, e.g., GENN and NOSMOG, employ positional embeddings to leverage structural information, further optimizing $I(\boldsymbol{A};\boldsymbol{y}_i)$ based on GLNN, but these methods only consider the *pure* graph structures.

SIMMLP employs self-supervised learning to maximize the mutual information between GNNs and MLPs (Bachman et al., 2020). The overall objective is to maximize $\sum_{i\in\mathcal{V}} I(\boldsymbol{y}_i;\boldsymbol{x}_i) + I(\boldsymbol{x}_i;\mathcal{S}_i)$. The first term optimizes the model on downstream tasks, corresponding to task-specific prediction head. The second term is the training objective of SIMMLP (Equation 4) that denotes the alignment between GNNs and MLPs. We argue, when the second term is maximized, $\boldsymbol{x}_i$ would preserve all knowledge of $\mathcal{S}_i$, turning the overall objective to maximize $\sum_{i\in\mathcal{V}} I(\boldsymbol{y}_i;\mathcal{S}_i)$. This demonstrates the equivalence between SIMMLP (in the optimal case) and GNNs, showing the superiority of SIMMLP in leveraging graph structures for predictions compared to existing MLP-based methods. Our analysis aligns with Chen et al. (2021) and Zhang et al. (2022) that the expressiveness of MLPs on node classification task is bounded by the induced ego-graphs $\mathcal{S}_i$.

4.2. Information Bottleneck Principle

Information bottleneck (Tishby et al., 2000; Tishby & Zaslavsky, 2015) is a principle in information theory, which focuses on compressing the observed random variables into the most informative and minimum compressions. For example, given a random variable $\boldsymbol{X}$ sampled from latent variable $\boldsymbol{Y}$, the aim is to find the optimal compression $\boldsymbol{Z}^* = \arg\min_{\boldsymbol{Z}} I(\boldsymbol{X};\boldsymbol{Z}) - \beta I(\boldsymbol{Z};\boldsymbol{Y})$. Intuitively, minimizing $I(\boldsymbol{X};\boldsymbol{Z})$ aims to obtain the minimum compression, and maximizing $I(\boldsymbol{Z};\boldsymbol{Y})$ preserves the essential information of $\boldsymbol{Y}$. Thus, the optimal compression $\boldsymbol{Z}^*$ would be informative and generalizable by eliminating latent variable-agnostic noise (Shwartz-Ziv & Tishby, 2017). For SIMMLP, we assume the observed graph $\mathcal{G}$ is sampled from latent graph $\mathcal{G}_{\mathcal{I}}$ (Proposition 3.1), and aim to compress the graph into $\boldsymbol{T} = (\boldsymbol{H}^{MLP}, \boldsymbol{H}^{GNN})$.

Proposition 4.2. *The optimal compression $\boldsymbol{T}^*$ satisfies*

$$\boldsymbol{T}^* = \arg\min_{\boldsymbol{H}^{MLP},\boldsymbol{H}^{GNN}} \lambda H(\boldsymbol{H}^{MLP}|\mathcal{G}_{\mathcal{I}}) + H(\boldsymbol{H}^{GNN}) + \lambda H(\boldsymbol{H}^{GNN}|\mathcal{G}_{\mathcal{I}}) + H(\boldsymbol{H}^{MLP}|\boldsymbol{H}^{GNN}), \quad (9)$$

where $\lambda = \frac{\beta}{1-\beta} > 0$.

[3]Too strong augmentation may cause the trivial solution again by injecting additional noise (Jing et al., 2022).

Table 3. SIMMLP has two key inductive biases in GNNs, i.e., homophily and local structure importance, which could be measured by `smoothness` and `min-cut`, respectively. SIMMLP approaches or even surpasses GNNs in terms of these two metrics.

Methods	Smoothness↓						Min-Cut↑					
	Cora	Citeseer	PubMed	Computer	Photo	Avg.	Cora	Citeseer	PubMed	Computer	Photo	Avg.
Raw Node Feature	0.8221	0.7825	0.7342	0.5393	0.5399	0.6836	–	–	–	–	–	–
SAGE (Hamilton et al., 2017)	0.1132	0.1835	0.1426	0.1564	0.1089	0.1409	0.9243	0.9426	0.9177	0.8541	0.8721	0.9022
BGRL (Thakoor et al., 2022)	0.1553	0.1023	0.3326	0.2509	0.2031	0.2088	0.8847	0.9346	0.8556	0.8336	0.8493	0.8716
MLP (Zhang et al., 2022)	0.4633	0.4442	0.4853	0.4557	0.4317	0.4560	0.6663	0.8035	0.8625	0.7183	0.7467	0.7595
GLNN (Zhang et al., 2022)	0.2818	0.2684	0.4208	0.3549	0.3976	0.3447	0.8863	0.9162	0.7934	0.8038	0.8113	0.8422
NOSMOG (Tian et al., 2023)	0.2672	0.2301	0.3942	0.3056	**0.2773**	0.2949	0.9023	0.9317	0.8337	0.8384	0.8226	0.8657
SIMMLP (Ours)	**0.1964**	**0.1703**	**0.3604**	**0.2986**	0.2878	**0.2627**	**0.9335**	**0.9575**	**0.8863**	**0.9014**	**0.8604**	**0.9078**

The proof is presented in Appendix A.3. $I(\cdot;\cdot)$ and $H(\cdot)$ denote mutual information and entropy, respectively. Intuitively, the optimal compression (Equation 9) is attainable with the optimal encoder $\mathcal{E}^*$ (Equation 5). To be specific, minimizing conditional entropy $H(\boldsymbol{H}^{MLP}|\mathcal{G}_{\mathcal{I}})$ and $H(\boldsymbol{H}^{GNN}|\mathcal{G}_{\mathcal{I}})$ preserves the latent information in GNN and MLP embeddings, which can be instantiated as minimizing $\|\boldsymbol{H}^{MLP} - \boldsymbol{F}^*\|^2 + \|\boldsymbol{H}^{GNN} - \boldsymbol{F}^*\|^2$. In addition, the minimum conditional entropy $H(\boldsymbol{H}^{MLP}|\boldsymbol{H}^{GNN})$ denotes the alignment between GNN and MLP embeddings, which could be modeled as maximizing $\sum_i \mathrm{Cov}(\boldsymbol{H}_i^{MLP}, \boldsymbol{H}_i^{GNN})$. Furthermore, minimizing entropy $H(\boldsymbol{H}^{GNN})$ reduces the uncertainty of the GNN embeddings, which could be achieved by preserving more node feature information, i.e., minimizing $\|\mathcal{D}(\boldsymbol{H}^{GNN}) - \boldsymbol{X}\|^2$. The analysis bridges the information bottleneck and the objective function of SIMMLP, showing the potential in learning generalizable node embeddings (Alemi et al., 2017).

4.3. Inductive Bias

The success of GNNs derives from the structural learning capability, which is unavailable for MLP-based methods. However, as discussed before, SIMMLP (in the optimal case) has the same learning objective as GNNs. To further analyze their potential equivalence, we investigate whether SIMMLP and GNNs have similar inductive biases. We hypothesize SIMMLP has two key inductive biases, i.e., homophily philosophy and local structure importance. The homophily philosophy indicates that topologically close nodes (e.g., directly connected nodes) would have similar properties. To leverage the inductive bias, message-passing iteratively updates the target nodes using neighborhood information, enforcing close nodes have similar embeddings. However, MLP-based methods cannot (or only can partially) leverage this due to the lack of structural learning ability. To evaluate the homophily, we measure the distance between embeddings of directly connected nodes, which corresponds to *smoothness*. In particular, we instantiate this as Mean Average Distance (MAD) (Chen et al., 2020a):

$$\text{MAD} = \frac{\sum_{i\in\mathcal{V}}\sum_{j\in\mathcal{N}(i)}(\boldsymbol{h}_i^{MLP} - \boldsymbol{h}_j^{MLP})^2}{\sum_{i\in\mathcal{V}}\sum_{j\in\mathcal{N}(i)}\mathbf{1}}. \tag{10}$$

Intuitively, a low smoothness value indicates a high similarity between directly connected nodes, demonstrating the capability to leverage graph structural information (Hou et al., 2019). The analysis over five real-world graphs is presented in Table 3. Compared to GNNs, MLP-based methods fall short in reducing the distance between topologically close nodes, even for NOSMOG that utilizes *pure* graph structural information in making predictions. SIMMLP goes beyond these methods by aligning GNNs and MLPs in a more intricate embedding space, approaching to GNNs.

Another inductive bias, i.e., local structure importance, describes the local neighborhoods preserve the crucial information for predictions. Alternatively, it measures the alignment between localized structures and model predictions. GNNs utilize ego-graph information in making predictions, naturally emphasizing the localized structures, but MLPs generally take node features as input, failing to fully leverage structural information. We argue, this inductive bias corresponds to the philosophy of *Min-Cut* (Stoer & Wagner, 1997). Specifically, using predictions $\hat{\boldsymbol{Y}}$ to denote graph partitions, a high Min-Cut value indicates a high correlation between predictions and localized structures, as it implies high intra-partition connectivity and low inter-partition connectivity. We follow Shi & Malik (2000) to model the Min-Cut problem:

$$\text{Min-Cut} = tr(\hat{\boldsymbol{Y}}^T\boldsymbol{A}\hat{\boldsymbol{Y}})/tr(\hat{\boldsymbol{Y}}^T\boldsymbol{D}\hat{\boldsymbol{Y}}), \tag{11}$$

where $\boldsymbol{A}$ and $\boldsymbol{D}$ are adjacency matrix and diagonal node degree matrix, respectively. The analysis results are presented in Table 3. SIMMLP demonstrates an inductive bias towards local structure importance, evidenced by the optimal average Min-Cut result.

5. Experiments

5.1. Experimental Setup

Datasets and Baselines. We evaluate SIMMLP on ten public benchmark datasets for node classification, including Cora, Citeseer, Pubmed, Computer (Amazon-CS), Photo (Amazon-Photo), Coauthor-CS, Coauthor-Physics, WikiCS, Flickr, and Arxiv. We use a variety of baselines, including supervised GNNs, e.g., SAGE, GAT, SGC, APPNP; self-supervised methods, including DGI, MVGRL, GRACE, BGRL, GCA; and MLP learning methods, such as vanilla MLP, GraphMLP, GLNN, GENN, and the recent SOTA

Table 4. Node classification accuracy in transductive setting, where the overall best and the sub-category best are indicated by **bold** and underline, respectively. We report the mean and standard deviation of ten runs with different random seeds to alleviate randomness.

	Methods	Cora	Citeseer	PubMed	Computer	Photo	Co-CS	Co-Phys	Wiki-CS	Flickr	Arxiv
GNN	SAGE (Hamilton et al., 2017)	81.44±0.91	70.44±1.39	85.94±0.43	88.88±0.27	93.81±0.42	93.41±0.16	95.72±0.05	80.87±0.63	48.45±0.78	72.05±0.25
	GAT (Veličković et al., 2018)	82.33±1.17	68.89±1.47	84.73±0.43	89.92±0.48	91.94±0.44	91.98±0.32	95.08±0.15	79.97±0.56	51.38±0.16	71.79±0.40
	APPNP (Gasteiger et al., 2019)	75.48±1.57	68.09±1.20	84.60±0.30	87.41±0.27	93.37±0.47	94.62±0.21	95.44±0.12	79.10±0.31	47.53±0.29	71.01±0.24
	SGC (Wu et al., 2019)	81.80±0.88	68.96±1.63	85.28±0.32	89.31±0.62	92.74±0.43	94.02±0.20	94.78±0.20	81.06±0.55	51.75±0.24	69.95±0.35
GCL	DGI (Veličković et al., 2019)	82.31±0.60	71.81±0.73	76.78±0.70	79.98±0.19	91.60±0.21	92.22±0.53	94.50±0.04	76.42±0.55	46.88±0.13	70.13±0.15
	MVGRL (Hassani & Khasahmadi, 2020)	83.89±0.50	72.14±1.25	86.33±0.59	87.85±0.31	91.88±0.15	92.15±0.07	95.30±0.04	77.64±0.09	49.32±0.11	70.88±0.10
	GRACE (Zhu et al., 2020)	80.50±1.03	65.52±2.06	84.64±0.50	88.44±0.33	92.83±0.56	93.01±0.30	95.43±0.06	78.59±0.47	49.33±0.11	70.96±0.13
	GCA (Zhu et al., 2021)	83.53±0.49	71.33±0.15	86.03±0.37	87.42±0.30	92.61±0.21	93.06±0.03	95.72±0.03	78.35±0.05	49.03±0.07	70.90±0.08
	BGRL (Thakoor et al., 2022)	81.30±0.59	66.90±0.58	84.92±0.24	88.19±0.21	92.54±0.11	92.11±0.12	95.21±0.07	77.54±0.79	49.67±0.06	70.84±0.12
MLP	MLP (Zhang et al., 2022)	64.49±1.90	64.01±1.26	80.69±0.28	80.79±0.33	87.77±0.49	91.65±0.32	95.11±0.12	75.16±0.46	46.21±0.07	56.44±0.30
	GraphMLP (Hu et al., 2021)	79.50±0.81	72.10±0.48	84.27±0.23	84.01±0.58	90.90±1.03	90.36±0.64	93.51±0.15	76.39±0.53	46.25±0.21	63.36±0.18
	GLNN (Zhang et al., 2022)	81.32±1.15	71.15±0.71	86.34±0.46	87.47±0.60	93.87±0.31	94.16±0.21	95.40±0.07	80.66±0.74	46.18±0.19	64.03±0.51
	GENN (Wang et al., 2023)	82.13±0.77	71.42±1.31	86.28±0.31	87.12±0.55	93.64±0.65	93.82±0.29	95.45±0.05	80.48±0.74	46.35±0.34	70.13±0.60
	NOSMOG (Tian et al., 2023)	82.27±1.13	72.39±1.27	86.18±0.33	87.64±1.14	93.94±0.47	93.83±0.23	95.74±0.12	80.53±0.77	46.69±0.25	70.84±0.44
	SIMMLP (Ours)	**84.60**±0.24	**73.52**±0.53	**86.99**±0.09	**88.46**±0.16	**94.28**±0.08	**94.87**±0.07	**96.17**±0.03	**81.21**±0.13	**49.85**±0.09	**71.12**±0.10

NOSMOG. More evaluation protocols are in Appendix B. Following we present three settings used in the experiment.

Transductive Setting. Given a graph $\mathcal{G} = (\mathcal{V}, E)$, all nodes $v \in \mathcal{V}$ are visible during training. In particular, the nodes are partitioned into three non-overlapping sets: $\mathcal{V} = \mathcal{V}_{train} \sqcup \mathcal{V}_{val} \sqcup \mathcal{V}_{test}$. For supervised models, we train the model on $\mathcal{V}_{train}$ and evaluate on $\mathcal{V}_{val}$ and $\mathcal{V}_{test}$. For self-supervised models, the encoder is pre-trained on all nodes $\mathcal{V}$; the prediction head is trained on $\mathcal{V}_{train}$ and evaluated on $\mathcal{V}_{val}$ and $\mathcal{V}_{test}$. We randomly split the node set 10 times for each seed to further alleviate the impact of randomness.

Inductive (Production) Setting. we randomly partition a graph $\mathcal{G} = (\mathcal{V}, E)$ into two non-overlapping subgraphs, namely transductive graph $\mathcal{G}^T = (\mathcal{V}^T, E^T)$ and inductive graph $\mathcal{G}^I = (\mathcal{V}^I, E^I)$. The transductive graph $\mathcal{G}^T$ is used for training, which contains 80% nodes; the inductive graph $\mathcal{G}^I$ is unseen during training, containing the remaining 20% nodes. We train the model on $\mathcal{G}^T$ as the transductive setting, which further partitions nodes in $\mathcal{G}^T$ as $\mathcal{V}^T = \mathcal{V}^T_{train} \sqcup \mathcal{V}^T_{valid} \sqcup \mathcal{V}^T_{test}$. We report three measures in total: (1) *transductive result* that is evaluated over $\mathcal{V}^T_{test}$, (2) *inductive result* that is evaluated over $\mathcal{V}^I$, and (3) *production result* that is the weighted average of the previous two. Compared to (Zhang et al., 2022; Tian et al., 2023), our setting is more challenging in that $\mathcal{V}^I$ is disconnected from $\mathcal{V}^T$ during the inference.

Cold-Start Setting. We randomly partition a graph $\mathcal{G} = (\mathcal{V}, E)$ into transductive graph $\mathcal{G}^T$ and inductive graph $\mathcal{G}^I$, and train the model as inductive setting. The only difference is nodes in $\mathcal{G}^I$ are isolated (removing all edges), that $\mathcal{G}^I = (\mathcal{V}^I, \emptyset)$. This aligns with real applications that new users commonly emerge independently (Hao et al., 2021). We report the performance on $\mathcal{V}^I$ as the cold-start result.

5.2. Node Classification

Table 4 reports the transductive node classification results. SIMMLP outperforms self-supervised GCL methods in all settings and supervised GNNs in 7 out of 10 datasets. Compared to MLP-based methods, SIMMLP surpasses MLP, GraphMLP, and GLNN on large-scaled Arxiv by 26%, 12%, and 11% improvements. In addition, SIMMLP achieves superior performance compared to GENN and state-of-the-art NOSMOG that explicitly encodes topological information. This shows the superiority of alignment in the embedding space in encoding fine-grained graph knowledge.

Table 5 presents the results of inductive setting. SIMMLP outperforms various baselines, demonstrating its potential deployment in real-world scenarios. Beyond our expectations, GLNN outperforms the advanced NOSMOG on 8 out of 10 datasets. It might be because the positional embeddings of NOSMOG learned from $\mathcal{G}^T$ and $\mathcal{G}^I$ are significantly distinct, hindering the model generalization.

Table 6 shows the results on the cold-start setting. SIMMLP achieves notable improvements over all baselines. In particular, SIMMLP obtains performance gain of 7% and 18% over vanilla MLP on Flickr and Arxiv, and 7% and 7% enhancements over NOSMOG. This demonstrates the superiority of modeling the fine-grained correlation between node features and graph structures in learning generalizable embeddings. This might enable the model to infer potential structural information based on the node feature itself. Additionally, the performance gain might also derive from augmentations, which provide more node-subgraph pairs during training. This can be evidenced by the unexpectedly high performance of BGRL, even though the model highly relies on structural information.

5.3. Inference Acceleration

We compare SIMMLP and other acceleration techniques on Flickr and Arxiv in inductive setting, as summarized in Table 7. We set SAGE as the backbone to implement three inference acceleration techniques (Zhang et al., 2022), including quantization (QSAGE), pruning (PSAGE), and neighbor sampling (Neighbor Sample). We also compare simplified SGC and APPNP that decompose feature trans-

Table 5. Node classification accuracy in inductive settings. Due to the space limitation, we only report the *production result*. The full results are presented in Appendix F (Table 15).

Methods	Cora	Citeseer	PubMed	Computer	Photo	Co-CS	Co-Phys	Wiki-CS	Flickr	Arxiv
SAGE (Hamilton et al., 2017)	77.51±1.77	68.40±1.61	85.04±0.44	87.24±0.43	93.20±0.45	92.88±0.40	95.74±0.12	79.26±0.65	47.17±0.73	68.52±0.56
BGRL (Thakoor et al., 2022)	77.73±1.07	64.33±1.56	83.97±0.48	87.33±0.48	91.47±0.62	91.26±0.35	94.38±0.29	76.25±1.09	49.12±0.31	69.29±0.38
MLP (Zhang et al., 2022)	63.76±1.65	63.98±1.22	80.91±0.45	81.00±0.54	87.73±0.88	91.68±0.59	95.18±0.13	75.08±0.71	46.14±0.22	55.89±0.51
GLNN (Zhang et al., 2022)	78.34±1.04	69.61±1.13	85.44±0.48	87.04±0.50	93.28±0.43	93.72±0.35	95.76±0.09	78.39±0.54	46.11±0.27	63.53±0.48
GENN (Wang et al., 2023)	77.83±1.57	67.30±1.48	84.34±0.47	85.75±1.20	92.09±0.96	93.57±0.37	95.67±0.06	78.27±1.01	45.56±0.51	68.52±0.54
NOSMOG (Tian et al., 2023)	77.83±1.94	68.58±1.41	83.84±0.45	86.61±1.22	92.52±0.68	93.45±0.44	95.78±0.10	78.35±0.70	46.05±0.55	69.10±0.80
SIMMLP (Ours)	**81.37**±1.20	**72.33**±0.90	**86.47**±0.28	**87.65**±0.40	**93.87**±0.32	**94.63**±0.16	**96.04**±0.12	**79.26**±0.83	**49.27**±0.18	**70.23**±0.47

Table 6. Node classification accuracy under cold-start setting.

Methods	Cora	Citeseer	PubMed	Computer	Photo	Co-CS	Co-Phys	Wiki-CS	Flickr	Arxiv
SAGE (Hamilton et al., 2017)	60.23±5.03	56.62±5.10	77.98±1.53	61.01±4.51	59.52±8.02	91.30±0.84	94.64±0.88	52.73±7.93	41.06±2.25	43.47±2.53
BGRL (Thakoor et al., 2022)	78.80±1.14	65.10±2.08	84.18±0.80	86.13±0.76	90.39±0.30	90.23±0.48	94.06±0.28	78.15±1.17	48.73±0.13	64.11±0.20
MLP (Zhang et al., 2022)	64.15±2.11	64.43±1.76	80.90±0.72	80.80±0.91	87.88±0.96	91.78±0.81	95.16±0.18	74.94±1.81	46.09±0.50	55.91±0.69
GLNN (Zhang et al., 2022)	71.96±1.68	69.14±2.58	84.42±0.87	83.98±0.70	91.05±0.49	93.34±0.47	95.70±0.09	77.64±1.42	46.05±0.43	60.55±0.55
GENN (Wang et al., 2023)	69.06±4.80	65.44±2.33	78.19±2.08	79.44±1.66	90.18±0.62	93.54±0.55	95.55±0.25	67.31±1.66	45.24±0.72	61.30±0.59
NOSMOG (Tian et al., 2023)	70.69±2.45	68.03±2.79	81.48±1.30	81.95±1.04	91.15±0.88	93.63±0.42	95.54±0.40	68.49±3.61	46.07±0.30	61.64±0.93
SIMMLP (Ours)	**80.48**±2.15	**72.81**±1.61	**86.44**±0.51	**87.58**±0.99	**93.91**±0.58	**94.51**±0.15	**95.97**±0.24	**78.46**±1.48	**49.41**±0.46	**66.13**±1.05

Table 7. Comparison between SIMMLP and acceleration methods in terms of inference time and accuracy under inductive setting.

	Flickr		Arxiv	
Methods	Time (ms)	Acc.	Time (ms)	Acc.
SAGE (Hamilton et al., 2017)	80.7	47.2	314.7	68.5
SGC (Wu et al., 2019)	76.9 (1.1×)	47.4	265.9 (1.2×)	68.9
APPNP (Gasteiger et al., 2019)	78.1 (1.0×)	47.5	284.1 (1.1×)	69.1
QSAGE (Zhang et al., 2022)	70.6 (1.1×)	47.2	289.5 (1.1×)	68.5
PSAGE (Zhang et al., 2022)	67.4 (1.2×)	47.3	297.5 (1.1×)	68.6
Neighbor Sample (Zhang et al., 2022)	25.5 (3.2×)	47.0	78.3 (4.0×)	68.4
SIMMLP (Ours)	**0.9 (89.7×)**	**49.3**	**2.5 (125.9×)**	**70.2**

formation and message-passing for fast inference. Even the most efficient technique only achieves marginal acceleration ($3.2 \sim 4.0\times$), and inevitably sacrifices model performance. SIMMLP achieves remarkable inference acceleration ($89.7 \sim 125.9\times$) by disregarding neighborhood fetching process. Compared to MLP-based methods, there are no significant differences in terms of inference speed ($\leq$ 2ms). However, some methods (Wang et al., 2023; Tian et al., 2023) may introduce additional time consumption in learning positional embeddings, which might takes $\sim$1s on large-scaled graphs.

Figure 3 demonstrates the trade-off between model performance and inference time on Arxiv with cold-start setting. SIMMLP achieves significant performance gain compared to MLP-based methods, and remarkable inference acceleration compared to GNN-based methods, showing the best trade-off. In addition, we observe more hidden dimensions can preserve more task-specific information for MLP-based methods, aligning to Zhang et al. (2022).

5.4. Extensive Experiments

SIMMLP exhibits robustness to noise in graph data and performs effectively with sparse labels (Appendix C). This aligns with practical scenarios where data is often noisy and label acquisition is challenging. In addition, SIMMLP can be readily employed to graph classification tasks and achieve desirable performance (Appendix G). Apart from the significant inference acceleration, it is efficient regarding training time and memory usage (Appendix D). We also present a comprehensive ablation study in Appendix E and the extension to supervised version in Appendix H.

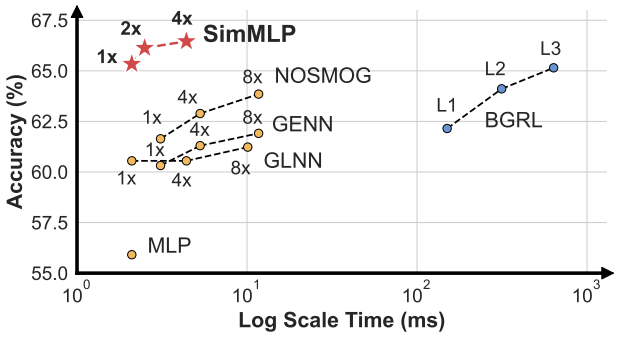

Figure 3. Accuracy vs. Inference Time on Arxiv under cold-start setting. The $k\times$ indicates the k times wider dimensions and L indicates the model layer.

6. Conclusion

We analyze existing MLP learning methods, distilling knowledge from GNNs, cannot generalize well to unseen nodes, and propose SIMMLP to solve it. The insight behind is that modeling the fine-grained correlation between node features and graph structures preserves generalizable information. To instantiate this, we apply self-supervised alignment between GNNs and MLPs in the embedding space. We theoretically show the equivalence between SIMMLP (in the optimal case) and GNNs in terms of the learning objective, and analyze its generalization capability and inductive bias. Experimental results show the effectiveness of SIMMLP especially for unseen nodes.

Boarder Impact

SIMMLP has positive impacts on graph learning community. This encourages the deployment of graph learning methods on latency-sensitive applications, such as financial fraud detection, where label acquisition is challenging and data is noisy, and with a lot of unseen nodes during the inference. We hope our work can inspire researchers seeking to develop novel learning paradigms on graphs that go beyond the scope of GNNs. There are no ethical concerns in the paper.

References

Alemi, A. A., Fischer, I., Dillon, J. V., and Murphy, K. Deep variational information bottleneck. In *ICLR*, 2017.

Bachman, P., Hjelm, R. D., and Buchwalter, W. Learning representations by maximizing mutual information across views. In *NeurIPS*, 2020.

Batson, J. and Royer, L. Noise2self: Blind denoising by self-supervision. In *ICML*, 2019.

Belghazi, M. I., Baratin, A., Rajeshwar, S., Ozair, S., Bengio, Y., Courville, A., and Hjelm, D. Mutual information neural estimation. In *ICML*, 2018.

Boudiaf, M., Rony, J., Ziko, I. M., Granger, E., Pedersoli, M., Piantanida, P., and Ayed, I. B. A unifying mutual information view of metric learning: cross-entropy vs. pairwise losses. In *ECCV*, 2020.

Cabannes, V., Kiani, B., Balestriero, R., LeCun, Y., and Bietti, A. The ssl interplay: Augmentations, inductive bias, and generalization. In *ICML*, 2023.

Caron, M., Bojanowski, P., Joulin, A., and Douze, M. Deep clustering for unsupervised learning of visual features. In *ECCV*, 2018.

Caron, M., Misra, I., Mairal, J., Goyal, P., Bojanowski, P., and Joulin, A. Unsupervised learning of visual features by contrasting cluster assignments. *NeurIPS*, 2020.

Chen, D., Lin, Y., Li, W., Li, P., Zhou, J., and Sun, X. Measuring and relieving the over-smoothing problem for graph neural networks from the topological view. In *AAAI*, 2020a.

Chen, L., Chen, Z., and Bruna, J. On graph neural networks versus graph-augmented MLPs. In *ICLR*, 2021.

Chen, T., Kornblith, S., Norouzi, M., and Hinton, G. A simple framework for contrastive learning of visual representations. In *ICML*, 2020b.

Chen, T., Kornblith, S., Swersky, K., Norouzi, M., and Hinton, G. E. Big self-supervised models are strong semi-supervised learners. *NeurIPS*, 2020c.

Ding, M., Kong, K., Li, J., Zhu, C., Dickerson, J., Huang, F., and Goldstein, T. VQ-GNN: A universal framework to scale up graph neural networks using vector quantization. In *NeurIPS*, 2021.

Dong, W., Wu, J., Luo, Y., Ge, Z., and Wang, P. Node representation learning in graph via node-to-neighbourhood mutual information maximization. In *CVPR*, 2022.

Dwivedi, V. P., Luu, A. T., Laurent, T., Bengio, Y., and Bresson, X. Graph neural networks with learnable structural and positional representations. In *ICLR*, 2022.

Frankle, J. and Carbin, M. The lottery ticket hypothesis: Finding sparse, trainable neural networks. In *ICLR*, 2019.

Gasteiger, J., Bojchevski, A., and Günnemann, S. Combining neural networks with personalized pagerank for classification on graphs. In *ICLR*, 2019.

Gilmer, J., Schoenholz, S. S., Riley, P. F., Vinyals, O., and Dahl, G. E. Neural message passing for quantum chemistry. In *ICML*, 2017.

Grill, J.-B., Strub, F., Altché, F., Tallec, C., Richemond, P., Buchatskaya, E., Doersch, C., Avila Pires, B., Guo, Z., Gheshlaghi Azar, M., et al. Bootstrap your own latent-a new approach to self-supervised learning. In *NeurIPS*, 2020.

Guo, Z., Shiao, W., Zhang, S., Liu, Y., Chawla, N. V., Shah, N., and Zhao, T. Linkless link prediction via relational distillation. In *ICML*, 2023.

Gupta, S., Agrawal, A., Gopalakrishnan, K., and Narayanan, P. Deep learning with limited numerical precision. In *ICML*, 2015.

Hamilton, W., Ying, Z., and Leskovec, J. Inductive representation learning on large graphs. In *NeurIPS*, 2017.

Han, S., Pool, J., Tran, J., and Dally, W. Learning both weights and connections for efficient neural network. In *NeurIPS*, 2015.

Han, X., Zhao, T., Liu, Y., Hu, X., and Shah, N. MLPInit: Embarrassingly simple GNN training acceleration with MLP initialization. In *ICLR*, 2023.

Hao, B., Zhang, J., Yin, H., Li, C., and Chen, H. Pre-training graph neural networks for cold-start users and items representation. In *WSDM*, 2021.

Hassani, K. and Khasahmadi, A. H. Contrastive multi-view representation learning on graphs. In *ICML*, 2020.

He, K., Fan, H., Wu, Y., Xie, S., and Girshick, R. Momentum contrast for unsupervised visual representation learning. In *CVPR*, 2020.

Hendrycks, D., Mazeika, M., Kadavath, S., and Song, D. Using self-supervised learning can improve model robustness and uncertainty. In *NeurIPS*, 2019.

Hinton, G., Vinyals, O., and Dean, J. Distilling the knowledge in a neural network. *arXiv*, 2015.

Hou, Y., Zhang, J., Cheng, J., Ma, K., Ma, R. T., Chen, H., and Yang, M.-C. Measuring and improving the use of graph information in graph neural networks. In *ICLR*, 2019.

Hou, Z., Liu, X., Cen, Y., Dong, Y., Yang, H., Wang, C., and Tang, J. Graphmae: Self-supervised masked graph autoencoders. In *KDD*, 2022.

Hu, W., Fey, M., Zitnik, M., Dong, Y., Ren, H., Liu, B., Catasta, M., and Leskovec, J. Open graph benchmark: Datasets for machine learning on graphs. In *NeurIPS*, 2020.

Hu, Y., You, H., Wang, Z., Wang, Z., Zhou, E., and Gao, Y. Graph-mlp: Node classification without message passing in graph. *arXiv*, 2021.

Huang, W., Yi, M., Zhao, X., and Jiang, Z. Towards the generalization of contrastive self-supervised learning. In *ICLR*, 2023.

Jacob, B., Kligys, S., Chen, B., Zhu, M., Tang, M., Howard, A., Adam, H., and Kalenichenko, D. Quantization and training of neural networks for efficient integer-arithmetic-only inference. In *CVPR*, 2018.

Jing, L., Vincent, P., LeCun, Y., and Tian, Y. Understanding dimensional collapse in contrastive self-supervised learning. In *ICLR*, 2022.

Kipf, T. N. and Welling, M. Semi-supervised classification with graph convolutional networks. In *ICLR*, 2017.

Lee, H., Hwang, S. J., and Shin, J. Self-supervised label augmentation via input transformations. In *ICML*, 2020.

Li, G., Muller, M., Thabet, A., and Ghanem, B. Deepgcns: Can gcns go as deep as cnns? In *ICCV*, 2019.

Lin, T.-Y., Goyal, P., Girshick, R., He, K., and Dollár, P. Focal loss for dense object detection. In *ICCV*, 2017.

Liu, S., Ounis, I., and Macdonald, C. An MLP-based algorithm for efficient contrastive graph recommendations. In *SIGIR*, 2022.

Mernyei, P. and Cangea, C. Wiki-cs: A wikipedia-based benchmark for graph neural networks. *arXiv*, 2020.

Morris, C., Kriege, N. M., Bause, F., Kersting, K., Mutzel, P., and Neumann, M. Tudataset: A collection of benchmark datasets for learning with graphs. *arXiv*, 2020.

Muthén, B. Latent variable analysis. *The Sage handbook of quantitative methodology for the social sciences*, 2004.

Narayanan, A., Chandramohan, M., Venkatesan, R., Chen, L., Liu, Y., and Jaiswal, S. graph2vec: Learning distributed representations of graphs. *arXiv*, 2017.

Shchur, O., Mumme, M., Bojchevski, A., and Günnemann, S. Pitfalls of graph neural network evaluation. *arXiv*, 2018.

Shervashidze, N., Schweitzer, P., Van Leeuwen, E. J., Mehlhorn, K., and Borgwardt, K. M. Weisfeiler-lehman graph kernels. *JMLR*, 2011.

Shi, J. and Malik, J. Normalized cuts and image segmentation. *TPAMI*, 2000.

Shwartz-Ziv, R. and Tishby, N. Opening the black box of deep neural networks via information. *arXiv*, 2017.

Stoer, M. and Wagner, F. A simple min-cut algorithm. *Journal of the ACM*, 1997.

Sun, F.-Y., Hoffman, J., Verma, V., and Tang, J. Infograph: Unsupervised and semi-supervised graph-level representation learning via mutual information maximization. In *ICLR*, 2020.

Sun, S., Cheng, Y., Gan, Z., and Liu, J. Patient knowledge distillation for bert model compression. In *EMNLP*, 2019.

Sun, X., Cheng, H., Li, J., Liu, B., and Guan, J. All in one: Multi-task prompting for graph neural networks. In *KDD*, 2023.

Thakoor, S., Tallec, C., Azar, M. G., Azabou, M., Dyer, E. L., Munos, R., Veličković, P., and Valko, M. Large-scale representation learning on graphs via bootstrapping. In *ICLR*, 2022.

Tian, Y., Krishnan, D., and Isola, P. Contrastive representation distillation. In *ICLR*, 2020a.

Tian, Y., Sun, C., Poole, B., Krishnan, D., Schmid, C., and Isola, P. What makes for good views for contrastive learning? *NeurIPS*, 2020b.

Tian, Y., Zhang, C., Guo, Z., Zhang, X., and Chawla, N. Learning MLPs on graphs: A unified view of effectiveness, robustness, and efficiency. In *ICLR*, 2023.

Tishby, N. and Zaslavsky, N. Deep learning and the information bottleneck principle. In *ITW*, 2015.

Tishby, N., Pereira, F. C., and Bialek, W. The information bottleneck method. *arXiv*, 2000.

Veličković, P., Cucurull, G., Casanova, A., Romero, A., Liò, P., and Bengio, Y. Graph attention networks. In *ICLR*, 2018.

Veličković, P., Fedus, W., Hamilton, W. L., Liò, P., Bengio, Y., and Hjelm, R. D. Deep graph infomax. In *ICLR*, 2019.

Wang, X., Lyu, D., Li, M., Xia, Y., Yang, Q., Wang, X., Wang, X., Cui, P., Yang, Y., Sun, B., et al. Apan: Asynchronous propagation attention network for real-time temporal graph embedding. In *SIGMOD*, 2021.

Wang, Y., Hooi, B., Liu, Y., and Shah, N. Graph explicit neural networks: Explicitly encoding graphs for efficient and accurate inference. In *WSDM*, 2023.

Weber, M., Domeniconi, G., Chen, J., Weidele, D. K. I., Bellei, C., Robinson, T., and Leiserson, C. E. Anti-money laundering in bitcoin: Experimenting with graph convolutional networks for financial forensics. *arXiv*, 2019.

Wu, F., Souza, A., Zhang, T., Fifty, C., Yu, T., and Weinberger, K. Simplifying graph convolutional networks. In *ICML*, 2019.

Xie, Y., Xu, Z., and Ji, S. Self-supervised representation learning via latent graph prediction. In *ICML*, 2022.

Xu, D., Cheng, W., Luo, D., Chen, H., and Zhang, X. Infogcl: Information-aware graph contrastive learning. In *NeurIPS*, 2021.

Xu, K., Hu, W., Leskovec, J., and Jegelka, S. How powerful are graph neural networks? In *ICLR*, 2019.

Yan, B., Wang, C., Guo, G., and Lou, Y. Tinygnn: Learning efficient graph neural networks. In *KDD*, 2020.

Yanardag, P. and Vishwanathan, S. Deep graph kernels. In *KDD*, 2015.

Yang, C., Liu, J., and Shi, C. Extract the knowledge of graph neural networks and go beyond it: An effective knowledge distillation framework. In *WWW*, 2021.

Yang, C., Wu, Q., Wang, J., and Yan, J. Graph neural networks are inherently good generalizers: Insights by bridging GNNs and MLPs. In *ICLR*, 2023a.

Yang, L., Tian, Y., Xu, M., Liu, Z., Hong, S., Qu, W., Zhang, W., Cui, B., Zhang, M., and Leskovec, J. Vqgraph: Graph vector-quantization for bridging gnns and mlps. *arXiv*, 2023b.

Yang, Z., Cohen, W., and Salakhudinov, R. Revisiting semi-supervised learning with graph embeddings. In *ICML*, 2016.

You, Y., Chen, T., Sui, Y., Chen, T., Wang, Z., and Shen, Y. Graph contrastive learning with augmentations. In *NeurIPS*, 2020.

You, Y., Chen, T., Shen, Y., and Wang, Z. Graph contrastive learning automated. In *ICML*, 2021.

Zbontar, J., Jing, L., Misra, I., LeCun, Y., and Deny, S. Barlow twins: Self-supervised learning via redundancy reduction. In *ICML*, 2021.

Zeng, H., Zhou, H., Srivastava, A., Kannan, R., and Prasanna, V. Graphsaint: Graph sampling based inductive learning method. In *ICLR*, 2020.

Zhang, S., Liu, Y., Sun, Y., and Shah, N. Graph-less neural networks: Teaching old MLPs new tricks via distillation. In *ICLR*, 2022.

Zhao, T., Liu, Y., Neves, L., Woodford, O., Jiang, M., and Shah, N. Data augmentation for graph neural networks. In *AAAI*, 2021.

Zhou, H., Srivastava, A., Zeng, H., Kannan, R., and Prasanna, V. Accelerating large scale real-time gnn inference using channel pruning. In *VLDB*, 2021.

Zhu, Y., Xu, Y., Yu, F., Liu, Q., Wu, S., and Wang, L. Deep graph contrastive representation learning. *arXiv*, 2020.

Zhu, Y., Xu, Y., Yu, F., Liu, Q., Wu, S., and Wang, L. Graph contrastive learning with adaptive augmentation. In *WWW*, 2021.

A. Proof

A.1. Proof of Proposition 3.1

Proposition 3.1. *Suppose $\mathcal{G} = (\boldsymbol{A}, \boldsymbol{X})$ is sampled from a latent graph $\mathcal{G}_{\mathcal{I}} = (\boldsymbol{A}, \boldsymbol{F})$, $\mathcal{G} \sim P(\mathcal{G}_{\mathcal{I}})$, and $\boldsymbol{F}^*$ is the lossless compression of $\boldsymbol{F}$ that $\mathbb{E}[\boldsymbol{X}|\boldsymbol{A}, \boldsymbol{F}^*] = \boldsymbol{F}$. Let ρ be an identity projector, and $\lambda = 1, \gamma = 1$. The optimal MLP encoder $\mathcal{E}^*$ satisfies*

$$\begin{aligned}\mathcal{E}^* = \arg\min_{\mathcal{E}} \mathbb{E}\left[\left\|\boldsymbol{H}^{MLP} - \boldsymbol{F}^*\right\|^2 + \left\|\boldsymbol{H}^{GNN} - \boldsymbol{F}^*\right\|^2\right] \\ + \mathbb{E}\left[\left\|\mathcal{D}(\boldsymbol{H}^{GNN}) - \boldsymbol{X}\right\|^2\right] - 2\mathbb{E}_{\boldsymbol{F}^*}\left[\sum_i \mathrm{Cov}(\boldsymbol{H}_i^{MLP}, \boldsymbol{H}_i^{GNN})|\boldsymbol{F}^*\right].\end{aligned} \tag{12}$$

Proof. Consider $\mathcal{G} = (\boldsymbol{A}, \boldsymbol{X})$, where $\boldsymbol{X} \in \mathbb{R}^{N\times d}$ is derived from a latent graph $\mathcal{G}_{\mathcal{I}} = (\boldsymbol{A}, \boldsymbol{F})$ following a distribution $\mathcal{G} \sim P(\mathcal{G}_{\mathcal{I}})$, with $\boldsymbol{F} \in \mathbb{R}^{N\times d}$ representing the latent node semantics. Additionally, consider an encoder $\mathcal{E}$ and a decoder $\mathcal{D}$ implemented as fully-connected layers, ensuring l-Lipschitz continuity with respect to the l_2-norm, and a GNN encoder ϕ. This yields $\boldsymbol{H}^{MLP} = \mathcal{E}(\boldsymbol{X})$ with $\boldsymbol{H}^{MLP} \in \mathbb{R}^{N\times d'}$, and $\boldsymbol{H}^{GNN} = \phi(\boldsymbol{X}, \boldsymbol{A})$ with $\boldsymbol{H}^{GNN} \in \mathbb{R}^{N\times d'}$. Furthermore, $\boldsymbol{F}^* \in \mathbb{R}^{N\times d'}$ denotes the lossless compression of $\boldsymbol{F}$ that $\mathbb{E}[\boldsymbol{X}|\boldsymbol{A}, \boldsymbol{F}^*] = \boldsymbol{F}$. The Equation 4 can be rewritten as:

$$\mathcal{E}^* = \arg\min_{\mathcal{E}} \mathbb{E}\left\|\boldsymbol{H}^{MLP} - \boldsymbol{H}^{GNN}\right\|^2 + \left\|\mathcal{D}(\boldsymbol{H}^{GNN}) - \boldsymbol{X}\right\|^2 \tag{13}$$

$$= \arg\min_{\mathcal{E}} \mathbb{E}\left\|(\boldsymbol{H}^{MLP} - \boldsymbol{F}^*) - (\boldsymbol{H}^{GNN} - \boldsymbol{F}^*)\right\|^2 + \left\|\mathcal{D}(\boldsymbol{H}^{GNN}) - \boldsymbol{X}\right\|^2 \tag{14}$$

$$\begin{aligned}= \arg\min_{\mathcal{E}} \mathbb{E}\left[\left\|\boldsymbol{H}^{MLP} - \boldsymbol{F}^*\right\|^2 + \left\|\boldsymbol{H}^{GNN} - \boldsymbol{F}^*\right\|^2 + \left\|\mathcal{D}(\boldsymbol{H}^{GNN}) - \boldsymbol{X}\right\|^2\right] \\ - 2\mathbb{E}\left[\left\langle \boldsymbol{H}^{MLP} - \boldsymbol{F}^*, \boldsymbol{H}^{GNN} - \boldsymbol{F}^*\right\rangle\right]\end{aligned} \tag{15}$$

$$\begin{aligned}= \arg\min_{\mathcal{E}} \mathbb{E}\left[\left\|\boldsymbol{H}^{MLP} - \boldsymbol{F}^*\right\|^2 + \left\|\boldsymbol{H}^{GNN} - \boldsymbol{F}^*\right\|^2 + \left\|\mathcal{D}(\boldsymbol{H}^{GNN}) - \boldsymbol{X}\right\|^2\right] \\ - 2\mathbb{E}_{\boldsymbol{F}^*}\left[\sum_i \left(\boldsymbol{H}_i^{MLP} - \boldsymbol{F}_i^*\right)\left(\boldsymbol{H}_i^{GNN} - \boldsymbol{F}_i^*\right)|\boldsymbol{F}^*\right]\end{aligned} \tag{16}$$

$$\begin{aligned}= \arg\min_{\mathcal{E}} \mathbb{E}\left[\left\|\boldsymbol{H}^{MLP} - \boldsymbol{F}^*\right\|^2 + \left\|\boldsymbol{H}^{GNN} - \boldsymbol{F}^*\right\|^2 + \left\|\mathcal{D}(\boldsymbol{H}^{GNN}) - \boldsymbol{X}\right\|^2\right] \\ - 2\mathbb{E}_{\boldsymbol{F}^*}\left[\sum_i \mathrm{Cov}(\boldsymbol{H}_i^{MLP} - \boldsymbol{F}^*, \boldsymbol{H}_i^{GNN} - \boldsymbol{F}^*)|\boldsymbol{F}^*\right].\end{aligned} \tag{17}$$

$$\begin{aligned}= \arg\min_{\mathcal{E}} \mathbb{E}\left[\left\|\boldsymbol{H}^{MLP} - \boldsymbol{F}^*\right\|^2 + \left\|\boldsymbol{H}^{GNN} - \boldsymbol{F}^*\right\|^2 + \left\|\mathcal{D}(\boldsymbol{H}^{GNN}) - \boldsymbol{X}\right\|^2\right] \\ - 2\mathbb{E}_{\boldsymbol{F}^*}\left[\sum_i \mathrm{Cov}(\boldsymbol{H}_i^{MLP}, \boldsymbol{H}_i^{GNN})|\boldsymbol{F}^*\right].\end{aligned} \tag{18}$$

Then, with a bit of simple transformations, the Equation 18 can be expressed in the form of Equation 12. We explain these four terms in details. The first two terms $\left\|\boldsymbol{H}^{MLP} - \boldsymbol{F}^*\right\|^2$ and $\left\|\boldsymbol{H}^{GNN} - \boldsymbol{F}^*\right\|^2$ indicate the reconstruction errors of MLP embedding $\boldsymbol{H}^{MLP}$ and GNN embedding $\boldsymbol{H}^{GNN}$ on the latent variable $\boldsymbol{F}^*$, ensuring the invariance on the latent graph $\mathcal{G}_{\mathcal{I}}$. The third term $\left\|\mathcal{D}(\boldsymbol{H}^{GNN}) - \boldsymbol{X}\right\|^2$ reconstructs the node feature $\boldsymbol{X}$ using GNN embeddings $\boldsymbol{H}^{GNN}$, mitigating the risk of potential distribution shifts. The last term $-2\sum_i \mathrm{Cov}(\boldsymbol{H}_i^{MLP}, \boldsymbol{H}_i^{GNN})$ maximizes the covariance between GNN and MLP embeddings at each dimension, aligning GNNs and MLPs in the embedding space.

A.2. Proof of Lemma 4.1

Lemma 4.1. *Minimizing the cross-entropy $H(\boldsymbol{Y}; \hat{\boldsymbol{Y}}|\boldsymbol{X})$ is equivalent to maximizing the mutual information $I(\boldsymbol{X}; \boldsymbol{Y})$.*

Proof. We follow the paper (Boudiaf et al., 2020) to prove the lemma. We show the equivalence between these two terms by

expanding $H(\boldsymbol{Y};\hat{\boldsymbol{Y}}|\boldsymbol{X})$ and $I(\boldsymbol{X};\boldsymbol{Y})$. We first expand the mutual information as

$$I(\boldsymbol{X};\boldsymbol{Y}) = H(\boldsymbol{Y}) - H(\boldsymbol{Y}|\boldsymbol{X}). \tag{19}$$

Maximizing the mutual information $I(\boldsymbol{X};\boldsymbol{Y})$ indicates minimizing the conditional entropy $H(\boldsymbol{Y}|\boldsymbol{X})$. The entropy on the label $H(\boldsymbol{Y})$ is a constant, which can be ignored.

The cross-entropy $H(\boldsymbol{Y};\hat{\boldsymbol{Y}}|\boldsymbol{X})$ can be written as the combination of conditional entropy $H(\boldsymbol{Y}|\boldsymbol{X})$ and KL divergence $\mathcal{D}_{KL}(\boldsymbol{Y}\|\hat{\boldsymbol{Y}}|\boldsymbol{X})$:

$$\begin{aligned}
H(\boldsymbol{Y};\hat{\boldsymbol{Y}}|\boldsymbol{X}) &= -\sum_i (\boldsymbol{Y}_i|\boldsymbol{X}) \log(\hat{\boldsymbol{Y}}_i|\boldsymbol{X}) && (20)\\
&= -\sum_i (\boldsymbol{Y}_i|\boldsymbol{X}) \log(\boldsymbol{Y}_i|\boldsymbol{X}) + \sum_i (\boldsymbol{Y}_i|\boldsymbol{X}) \log(\boldsymbol{Y}_i|\boldsymbol{X}) - \sum_i \boldsymbol{Y}_i \log(\hat{\boldsymbol{Y}}_i|\boldsymbol{X}) && (21)\\
&= H(\boldsymbol{Y}|\boldsymbol{X}) + \sum_i (\boldsymbol{Y}_i|\boldsymbol{X}) \log \frac{(\boldsymbol{Y}_i|\boldsymbol{X})}{(\hat{\boldsymbol{Y}}_i|\boldsymbol{X})} && (22)\\
&= H(\boldsymbol{Y}|\boldsymbol{X}) + \mathcal{D}_{KL}(\boldsymbol{Y}\|\hat{\boldsymbol{Y}}|\boldsymbol{X}) && (23)
\end{aligned}$$

Considering Equation 23, minimizing the cross-entropy $H(\boldsymbol{Y};\hat{\boldsymbol{Y}}|\boldsymbol{X})$ can minimize $H(\boldsymbol{Y}|\boldsymbol{X})$ (as well as $\mathcal{D}_{KL}(\boldsymbol{Y}\|\hat{\boldsymbol{Y}}|\boldsymbol{X})$), which is equivalent to maximizing the mutual information $I(\boldsymbol{X};\boldsymbol{Y})$. Based on the analysis in (Boudiaf et al., 2020), Equation 23 can be optimized in a *Max-Min* manner. In particular, the first step is to freeze the encoder and only optimize the classifier, corresponding to fix $H(\boldsymbol{Y}|\boldsymbol{X})$ and minimize $\mathcal{D}_{KL}(\boldsymbol{Y}\|\hat{\boldsymbol{Y}}|\boldsymbol{X})$. The KL term would ideally vanish at the end of this step. Following step involves optimizing the parameters of the encoder while fixing the classifier.

A.3. Proof of Proposition 4.2

Proposition 4.2. *The optimal compression $\boldsymbol{T}^*$ satisfies*

$$\boldsymbol{T}^* = \underset{\boldsymbol{H}^{MLP},\boldsymbol{H}^{GNN}}{\arg\min}\ \lambda H(\boldsymbol{H}^{MLP}|\mathcal{G}_{\mathcal{I}}) + H(\boldsymbol{H}^{GNN}) + \lambda H(\boldsymbol{H}^{GNN}|\mathcal{G}_{\mathcal{I}}) + H(\boldsymbol{H}^{MLP}|\boldsymbol{H}^{GNN}), \tag{24}$$

where $\lambda = \frac{\beta}{1-\beta} > 0$, $I(\cdot;\cdot)$ denotes mutual information, and $H(\cdot)$ indicates entropy.

Proof. Before the proof, we need to provide some notations. We aim to compress the original graph $\mathcal{G}$ into $\boldsymbol{T} = (\boldsymbol{H}^{MLP}, \boldsymbol{H}^{GNN})$ by preserving the information of latent graph $\mathcal{G}_{\mathcal{I}}$. Based on the definition of information bottleneck (Tishby et al., 2000), the optimal compression is

$$\boldsymbol{T}^* = \arg\min_{\boldsymbol{T}} I(\mathcal{G};\boldsymbol{T}) - \beta I(\boldsymbol{T};\mathcal{G}_{\mathcal{I}}), \tag{25}$$

where β denotes the Lagrange multiplier and $I(\cdot;\cdot)$ is the mutual information. The optimal compression $\boldsymbol{T}^*$ preserves the essential latent information by maximizing $\beta I(\boldsymbol{T};\mathcal{G}_{\mathcal{I}})$ and discard the noises contained in the observed data $\mathcal{G}$ by minimizing $I(\mathcal{G};\boldsymbol{T})$. To handle the equation in a more accessible manner, we convert it as

$$\begin{aligned}
\boldsymbol{T}^* &= \arg\min_{\boldsymbol{T}} I(\mathcal{G};\boldsymbol{T}) - \beta I(\boldsymbol{T};\mathcal{G}_{\mathcal{I}}) && (26)\\
&= \arg\min_{\boldsymbol{T}} (1-\beta) H(\boldsymbol{T}) + \beta H(\boldsymbol{T}|\mathcal{G}_{\mathcal{I}}) - H(\boldsymbol{T}|\mathcal{G}) && (27)\\
&= \arg\min_{\boldsymbol{T}} H(\boldsymbol{T}) + \lambda H(\boldsymbol{T}|\mathcal{G}_{\mathcal{I}}) && (28)\\
&= \underset{\boldsymbol{H}^{MLP},\boldsymbol{H}^{GNN}}{\arg\min}\ \lambda H(\boldsymbol{H}^{MLP}|\mathcal{G}_{\mathcal{I}}) + H(\boldsymbol{H}^{GNN}) + \lambda H(\boldsymbol{H}^{GNN}|\mathcal{G}_{\mathcal{I}}) + H(\boldsymbol{H}^{MLP}|\boldsymbol{H}^{GNN}), && (29)
\end{aligned}$$

where $\lambda = \frac{\beta}{1-\beta} > 0$ and $H(\cdot)$ is the entropy.

B. Experimental Setup

In this section, we provide a comprehensive description of the experimental setup for node classification task. The experiments are conducted on Nvidia A100 (80GB) for the Arxiv dataset, and Nvidia GeForce RTX 3090 (24GB) for the remaining datasets.

B.1. Dataset Statistics

Table 8. The statistics of node classification datasets.

Dataset	Task	# Graphs	# Nodes	# Edges	# Features	# Classes	Split
Cora	Node-level	1	2,708	10,556	1,433	7	10%/10%/80%
Citeseer	Node-level	1	3,327	9,104	3,703	6	10%/10%/80%
PubMed	Node-level	1	19,717	88,648	500	3	10%/10%/80%
Computer	Node-level	1	13,752	491,722	767	10	10%/10%/80%
Photo	Node-level	1	7,650	238,162	745	8	10%/10%/80%
Co-CS	Node-level	1	18,333	163,788	6,805	15	10%/10%/80%
Co-Phys	Node-level	1	34,493	495,924	8,415	5	10%/10%/80%
Wiki-CS	Node-level	1	11,701	432,246	300	10	10%/10%/80%
Flickr	Node-level	1	89,250	899,756	500	7	10%/10%/80%
Arxiv	Node-level	1	169,343	1,166,243	128	40	Public Split

We select 10 benchmark datasets to evaluate the performance of SIMMLP and other baselines on node classifications. These datasets are collected from diverse domains, encompassing citation networks, social networks, wikipedia networks, etc. We present the statistics of these datasets in Table 8.

Specifically, **Cora, Citeseer, PubMed** (Yang et al., 2016) are three citation networks, in which nodes denote papers and edges represent citations. The node features are represented as bag-of-words based on paper keywords. **Computer (Amazon-CS) and Photo (Amazon-Photo)** (Shchur et al., 2018) are two co-purchase networks that describe the frequent co-purchases of items (nodes). **Co-CS (Coauthor-CS) and Co-Phys (Coauthor-physics)** (Shchur et al., 2018) consist of nodes representing authors and edges indicating collaborations between authors. **Wiki-CS** (Mernyei & Cangea, 2020) is extracted from Wikipedia, comprising computer science articles (nodes) connected by hyperlinks (edges). **Flickr** (Zeng et al., 2020) consists online images, with the goal of categorizing images based on their descriptions and common properties. All these datasets are available through PyG (Pytorch Geometric), and we partition them randomly into training, validation, and testing sets with a split ratio of 10%/10%/80%. Additionally, we employ **Arxiv** dataset from OGB benchmarks (Hu et al., 2020) to evaluate model performance on large-scale datasets. We process the dataset in PyG using OGB public interfaces with standard public split setting.

B.2. Summary of Baselines

We compare SIMMLP against a range of baselines, encompassing supervised GNNs, self-supervised graph contrastive learning (GCL) methods, and MLP-based graph learning methods.

Supervised GNNs. Our primary node classification baselines include **GraphSAGE** (Hamilton et al., 2017) and **GAT** (Veličković et al., 2018). Furthermore, we also incorporate **SGC** (Wu et al., 2019) and **APPNP** (Gasteiger et al., 2019) as additional node classification baselines.

Self-supervised GNNs. We compare SIMMLP to self-supervised graph learning methods. **DGI** (Veličković et al., 2019) and **MVGRL** (Hassani & Khasahmadi, 2020) conduct contrastive learning between graph patches and graph summaries to integrate knowledge into node embeddings. **GRACE** (Zhu et al., 2020) and subsequent **GCA** (Zhu et al., 2021) perform contrast between nodes in two corrupted views to acquire augmentation-invariant embeddings. **BGRL** (Thakoor et al., 2022) utilizes predictive objective for node-level contrastive learning to achieve efficient training.

MLPs on Graphs. In node classification, we employ basic **MLP** that considers only node content as baseline. Furthermore, we incorporate **GraphMLP** (Hu et al., 2021) that trains an MLP by emphasizing consistency between target nodes and their direct neighborhoods. We exclude the following works (Dong et al., 2022; Liu et al., 2022) as baselines since they are high-order versions of GraphMLP. To achieve this, we slightly modify the original GraphMLP to enable the ability in learning high-order information, and search the number of layers within $\{1, 2, 3\}$. **GLNN** (Zhang et al., 2022) employs

knowledge distillation to transfer knowledge from GNNs to MLPs, **GENN** leverages positional encoding to acquire structural knowledge, while **NOSMOG** (Tian et al., 2023) jointly integrates positional information and robust training strategies based on GLNN. Note that the public code of GENN is not available, thus we implement GENN based on the code of NOSMOG.

B.3. Hyper-parameter setting

Table 9. Hyper-parameters used for SIMMLP for node-level task.

	Node Classification									
Hyper-parameters	Cora	Citeseer	PubMed	Computer	Photo	Co-CS	Co-Phys	Wiki-CS	Flickr	Arxiv
Epochs	1000	1000	1000	1000	1000	2000	1000	2000	2000	5000
Optimizer	AdamW used for all datasets									
Learning Rate	1e-3	5e-4	5e-4	1e-3	1e-3	1e-4	1e-3	5e-4	1e-3	1e-3
Weight Decay	0	5e-5	1e-5	-	1e-4	-	1e-4	1e-5	5e-4	-
Activation	PReLU used for all datasets									
Hidden Dimension	512	512	512	512	512	512	512	512	1024	1024
Normalization	Batchnorm used for all datasets									
# MLP Layers	2	2	2	3	2	2	2	2	2	8
# GNN Layers	2	3	3	2	1	1	1	2	3	3
Feature Mask Ratio	0.50	0.75	0.25	0.25	0.25	0.50	0.75	0.00	0.25	0.00
Edge Mask Ratio	0.25	0.50	0.25	0.25	0.50	0.75	0.50	0.25	0.50	0.25

We perform hyper-parameter tuning for each approach using a grid search strategy. Specifically, we set the number of epochs to 1,000, the hidden dimension to 512, and employ PReLU as the activation function. We explore various learning rates {5e-4, 1e-4, 5e-4, 1e-3, 5e-3, 1e-2}, weight decay values {5e-5, 1e-5, 5e-3, 1e-4, 0}, and the number of layers {1, 2, 3}. In self-supervised learning methods, we employ a 2-layer GCN (Kipf & Welling, 2017) as the encoder for node-level tasks. Subsequently, we assess the quality of the acquired embeddings by training a Logistic regression function on downstream tasks (Zhu et al., 2020). For other settings, we follow the settings reported in the original papers. Regarding SIMMLP, we provide a comprehensive overview of the hyper-parameter settings for node classification task in Table 9.

C. Robustness Analysis

We analyze the model robustness on noisy data and sparse labels in this section. We apply the inductive setting and report the results on inductive graph $\mathcal{G}^I$. Figure 4 shows the experimental results averaged over seven datasets, including Cora, Citeseer, PubMed, Computer, Photo, Co-CS, and Wiki-CS.

Noisy Graph Structure. To inject structural noise, we randomly flip edges of the graph. Specifically, we replace $\boldsymbol{A}$ with $\tilde{\boldsymbol{A}} = \boldsymbol{M} \odot (1 - \boldsymbol{A}) + (1 - \boldsymbol{M}) \odot \boldsymbol{A}$, $\boldsymbol{M}_{ij} \sim \mathcal{B}(p)$, where $\mathcal{B}(p)$ is a Bernoulli distribution with probability p. The impact of structural noise is depicted in Figure 4 **(Left)**. Compared to other baselines, SIMMLP is not sensitive to structural noise even with extremely high noise ratios, demonstrating its robustness. We observe the impact of structural noise is marginal on MLPs (even $\tilde{\boldsymbol{A}}$ becomes independent to $\boldsymbol{A}$), but imposes significant performance degradation on GNNs, particularly for self-supervised BGRL. This might because the inference of GNNs highly relies on graph structures, where the slight modification would lead to significant distribution shift.

Noisy Node Features. We examine the impact of node feature noise by injecting random Gaussian noise. In particular, we replace $\boldsymbol{X}$ with $\tilde{\boldsymbol{X}} = (1 - \alpha)\boldsymbol{X} + \alpha x$, where x is random noise agnostic to $\boldsymbol{X}$, and $\alpha \in [0, 1]$ denotes noise level. As depicted in Figure 4 **(Middle)**, existing MLP-based methods degrades rapidly with the increase of noise levels, since the quality of node features is crucial for these methods (Zhang et al., 2022; Guo et al., 2023). However, SIMMLP still surpasses all baselines in all settings. We assume this robustness derives from the augmentation strategy that synthesizes additional high-quality node and ego-graph pairs, thereby aiding the training of MLP. The observation aligns with BGRL that also applies augmentation techniques.

Label Sparsity. In addition, we analyze the robustness of SIMMLP under label sparsity scenario, as shown in Figure 4 **(Right)**. Benefit from the nature of contrastive learning, SIMMLP consistently outperforms all other baselines, even with extremely limited training data (0.001). The benefit derives from the capability in leveraging unlabeled data during training,

while supervised methods may fall into over-fitting.

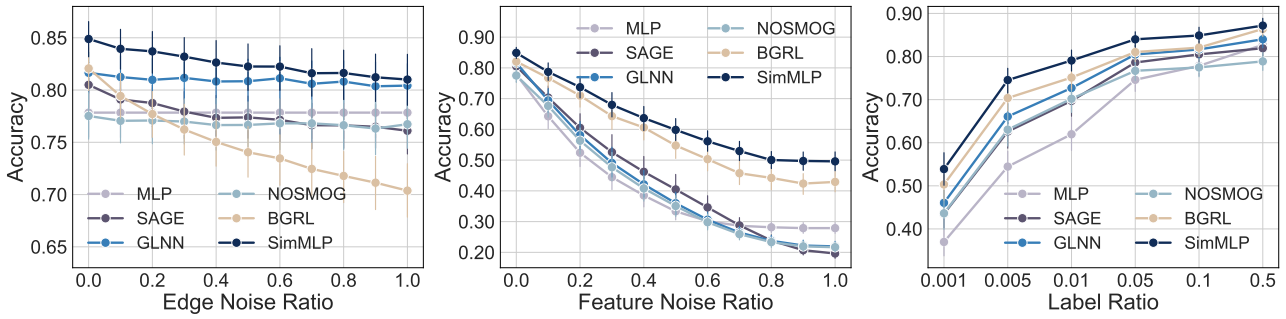

Figure 4. **Left**: Edge Noise. SIMMLP consistently demonstrates robustness against edge noise, even in scenarios with exceptionally high noise ratios. **Middle**: Feature Noise. SIMMLP demonstrates robustness to feature noise, whereas other MLP-based methods are susceptible to it. **Right**: Label Sparsity. SIMMLP significantly outperforms other baselines, especially with low label ratios.

D. Training Efficiency Analysis

Table 10 presents a comparison of the running time and memory usage between SIMMLP and other baselines, namely GAT (Veličković et al., 2018), GRACE (Zhu et al., 2020), and BGRL (Thakoor et al., 2022). Apart from the significant inference acceleration, SIMMLP has less training time and memory usage. In particular, GAT with 4 attention heads imposes a substantial computational consumption in model training. This is highly probable to be the consumption in learning attention scores. GRACE utilizes InfoNCE loss to align the consistency between two graph views, where the similarity measurements might lead to significant computational overhead. Compared to this method, SIMMLP demonstrates improvements in terms of memory usage ($3.8 \sim 6.8\times$) and training time ($4.8 \sim 8.3\times$). BGRL employs bootstrap (Grill et al., 2020) to alleviate the need for negative samples in InfoNCE, thus alleviating significant computational usage in measuring the distance between negative pairs. However, SIMMLP remains more efficient than BGRL due to the use of MLP encoder.

Table 10. Computational requirements of different baseline methods on a set of standard benchmark graphs. The experiments are performed on a 24GB Nvidia GeForce RTX 3090.

	Computer		Photo		Coauthor-CS		Coauthor-Phys		Wiki-CS	
Methods	Memory	Training Time	Memory	Training Time	Memory	Training Time	Memory	Training Time	Memory	Training Time
GAT	5239 MB	73.8 (s)	2571 MB	41.9 (s)	2539 MB	60.4 (s)	13199 MB	265.2 (s)	4568 MB	74.4 (s)
GRACE	8142 MB	349.5 (s)	2755 MB	138.4 (s)	11643 MB	261.4 (s)	16294 MB	573.2 (s)	5966 MB	290.9 (s)
BGRL	2196 MB	96.8 (s)	1088 MB	64.1 (s)	2513 MB	129.9 (s)	5556 MB	273.8 (s)	1899 MB	108.8 (s)
SIMMLP	**1969 MB**	**53.4 (s)**	**694 MB**	**27.0 (s)**	**1716 MB**	**54.8 (s)**	**3920 MB**	**110.7 (s)**	**1590 MB**	**35.5 (s)**

E. Comprehensive Ablation Study

E.1. The necessity in incorporating structural information

Table 11. The ablation study on incorporating structural information using GNNs. Without the GNN encoder (i.e., only using MLPs), the model performance will be significantly decreased.

Methods	Cora	Citeseer	PubMed	Computer	Photo	Co-CS	Co-Phys	Wiki-CS	Flickr	Arxiv
SIMMLP	**84.60**$_{\pm 0.24}$	**73.52**$_{\pm 0.53}$	**86.99**$_{\pm 0.09}$	**88.46**$_{\pm 0.16}$	**94.28**$_{\pm 0.08}$	**94.87**$_{\pm 0.07}$	**96.17**$_{\pm 0.03}$	**81.21**$_{\pm 0.13}$	**49.85**$_{\pm 0.09}$	**71.12**$_{\pm 0.10}$
w/o GNN	55.91$_{\pm 0.66}$	57.36$_{\pm 0.33}$	79.93$_{\pm 0.32}$	72.76$_{\pm 0.71}$	77.05$_{\pm 0.18}$	91.19$_{\pm 0.13}$	93.35$_{\pm 0.12}$	73.87$_{\pm 0.26}$	45.82$_{\pm 0.07}$	54.83$_{\pm 0.41}$

The use of GNN encoder in learning structure-aware knowledge is essential in SIMMLP, as it directly aligns the embeddings of two encoders. Without the GNN encoder, the model will fail to capture the fine-grained and generalizable correlation between node features and graph structures, demonstrated in Table 11.

E.2. Without Strategy 1 would lead to model collapse

See Figure 5.

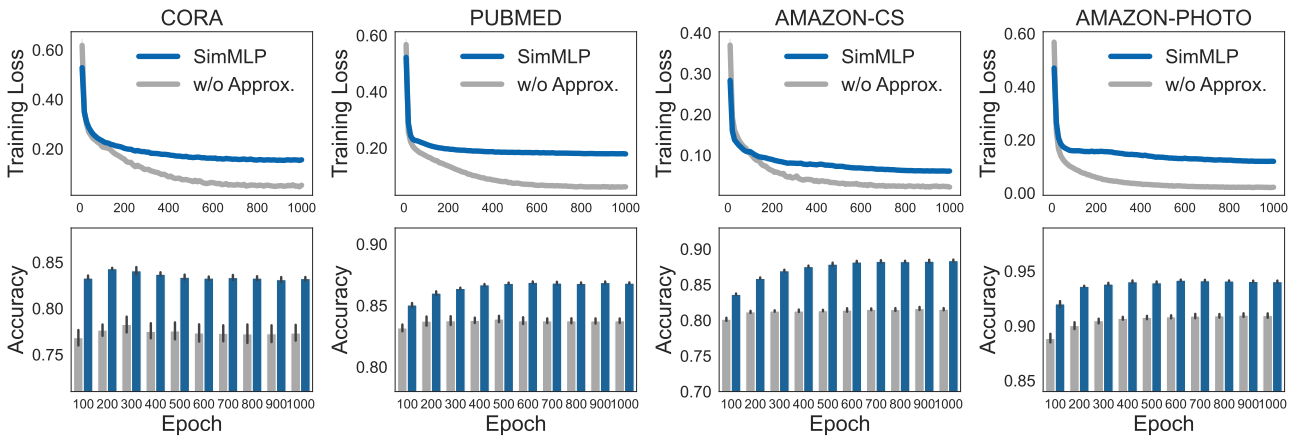

Figure 5. More results to show the effectiveness of Strategy 1 (Approx.) in preventing trivial solutions.

E.3. The design choice of Strategy 1

Table 12. Ablation study on node aggregation choices. `Col` indicates column-normalized Laplacian aggregation matrix $\tilde{\boldsymbol{D}}^{-1}\tilde{\boldsymbol{A}}$, `Row` indicates row-normalized Laplacian aggregation matrix $\tilde{\boldsymbol{A}}\tilde{\boldsymbol{D}}^{-1}$, and `Bi.` indicates bi-normalized Laplacian aggregation matrix $\tilde{\boldsymbol{D}}^{-1/2}\tilde{\boldsymbol{A}}\tilde{\boldsymbol{D}}^{-1/2}$. SIMMLP employs `Bi.` since it consistently outperforms others even though the improvements may not be significant.

	Cora	Citeseer	PubMed	Computer	Photo	Co-CS	Co-Phys	Wiki-CS	Flickr	Arxiv
`Bi.`	**84.60**$_{\pm 0.24}$	**73.52**$_{\pm 0.53}$	**86.99**$_{\pm 0.09}$	**88.46**$_{\pm 0.16}$	**94.28**$_{\pm 0.08}$	**94.87**$_{\pm 0.07}$	**96.17**$_{\pm 0.03}$	**81.21**$_{\pm 0.13}$	**49.85**$_{\pm 0.09}$	**71.12**$_{\pm 0.10}$
`Col`	84.14$_{\pm 0.34}$	73.48$_{\pm 0.53}$	86.92$_{\pm 0.08}$	87.93$_{\pm 0.27}$	93.11$_{\pm 0.15}$	94.81$_{\pm 0.06}$	96.09$_{\pm 0.03}$	80.62$_{\pm 0.30}$	49.15$_{\pm 0.16}$	71.03$_{\pm 0.09}$
`Row`	84.09$_{\pm 0.32}$	73.49$_{\pm 0.54}$	86.92$_{\pm 0.08}$	87.96$_{\pm 0.27}$	93.07$_{\pm 0.15}$	94.82$_{\pm 0.06}$	96.07$_{\pm 0.04}$	80.63$_{\pm 0.25}$	49.18$_{\pm 0.10}$	71.04$_{\pm 0.09}$

In this section, we analyze some design choices of Strategy 1, i.e., using MLP to approximate GNN. The learning process is similar to SGC (Wu et al., 2019) or APPNP (Gasteiger et al., 2019) that decompose feature transformation and message-passing. In SIMMLP, we consider using normalized Laplacian matrix to direct the message passing due to its simplicity. Based on the normalization, we have three design choices. We dub them as (1) `Col`: using column-normalized Laplacian matrix $\tilde{\boldsymbol{D}}^{-1}\tilde{\boldsymbol{A}}$ for message-passing, (2) `Row`: using row-normalized Laplacian matrix $\tilde{\boldsymbol{A}}\tilde{\boldsymbol{D}}^{-1}$ for message-passing, and (3) `Bi`: using bi-normalized Laplacian matrix $\tilde{\boldsymbol{D}}^{-1/2}\tilde{\boldsymbol{A}}\tilde{\boldsymbol{D}}^{-1/2}$ for message-passing. Here $\tilde{\boldsymbol{A}} = \boldsymbol{A} + \boldsymbol{I}$ and $\tilde{\boldsymbol{D}}$ is the diagonal matrix of node degrees of $\tilde{\boldsymbol{A}}$. We present the results of these three choices on ten benchmark datasets, shown in Table E.3.

In this table, we observe that there is no significant difference in performance among the various aggregation methods. All of these methods can achieve desirable performance. Nevertheless, the bi-normalized aggregation (`Bi.`) consistently outperforms the others. Actually, we can directly use the message-passing functions of SGC or APPNP. For SGC, we do not observe significant performance differences compared to the discussed three choices. For APPNP that performs message-passing based on page-rank, we consider obtaining the page-rank aggregation matrix would lead to significant time consumption, especially with graph structural augmentations. We leave this in the future work.

Apart from the choice of message-passing methods, determining the message-passing layers is also important. We show the performance of SIMMLP with varying numbers of message-passing layers on five benchmark datasets in Figure 6. We observe the optimal performance is achieved with 2 or 3 layers, which is consistent with prior research on GNNs (Li et al., 2019). It might be because a high number of message-passing layers can result in over-smoothing.

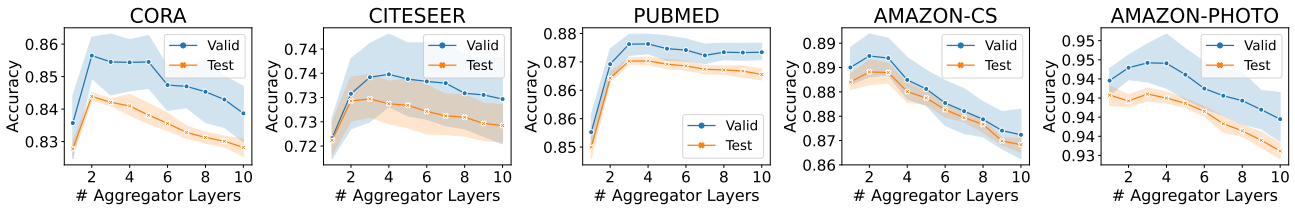

Figure 6. Node classification accuracy on transductive setting with different aggregation layers.

E.4. How does Strategy 2 (augmentation) prevent trivial solutions?

In this section, we evaluate the influence of augmentations on model performance. We conduct an ablation study to assess the model performance without specific augmentations, demonstrating both edge masking and node feature masking enhance model performance. Table 13 presents the results on ten benchmark datasets under the transductive setting. We observe that these two types of augmentations significantly enhance model performance by improving different aspects of the datasets. Furthermore, the combination of these two techniques further enhances the performance of SIMMLP, indicating that our model can benefit from both augmentations simultaneously.

Table 13. Ablation study of augmentation methods used in SIMMLP.

Feature Masking	Edge Masking	Cora	Citeseer	PubMed	Computer	Photo	Co-CS	Co-Phys	Wiki-CS	Flickr	Arxiv
-	-	82.10±0.45	71.83±0.43	86.89±0.13	87.12±0.15	93.52±0.20	93.10±0.05	94.56±0.06	80.98±0.13	48.21±0.10	70.58±0.20
√	-	84.78±0.25	73.00±0.63	86.98±0.09	88.27±0.18	94.19±0.14	94.50±0.10	96.12±0.06	81.03±0.11	49.55±0.11	70.03±0.23
-	√	82.33±0.61	71.78±0.77	86.98±0.13	87.35±0.29	93.69±0.07	94.35±0.08	95.88±0.06	81.04±0.22	49.33±0.07	**71.12±0.10**
√	√	**84.60±0.24**	**73.52±0.53**	**86.99±0.09**	**88.46±0.16**	**94.28±0.08**	**94.87±0.07**	**96.17±0.03**	**81.21±0.13**	**49.85±0.09**	**71.12±0.10**

Additionally, we conduct a detailed analysis of how augmentations impact model performance. Figure 7 illustrates the model performance at different augmentation probabilities on Cora, Citeseer, PubMed, Computer, and Photo datasets under the transductive setting. The augmentation ratio is searched among $\{0.0, 0.25, 0.5, 0.75\}$. These figures enable us to gain insight into the specific effects of augmentations on model performance.

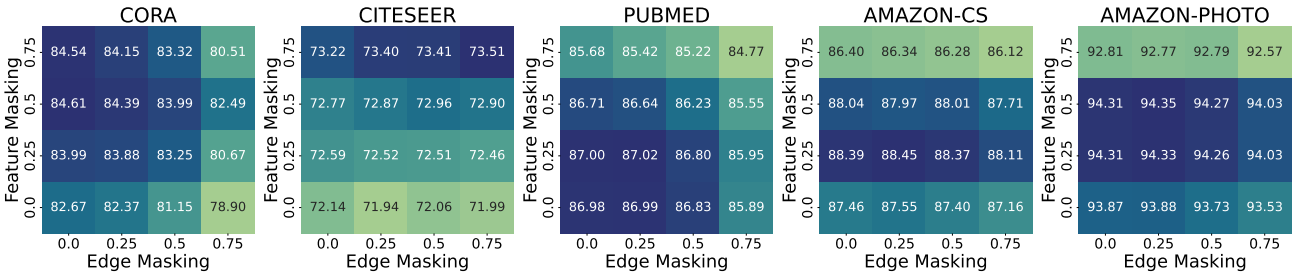

Figure 7. Node classification accuracy on transductive setting with different augmentation ratios.

E.5. How the reconstruction term in Equation 4 works?

In this section, we evaluate the role of the reconstruction term of SIMMLP in Equation 4. We treat the term serves as a regularizer that mitigates the potential distribution shifts. It works like positional embedding (Dwivedi et al., 2022) that preserves more localized information on GNN embeddings. We show the impact of the reconstruction term on model performance in Table 14. Our observations indicate the reconstruction term might be important in large-scale datasets, e.g., Arxiv. It might be because these datasets contain more noise.

Table 14. Reconstruction term in Equation 4 serves as a regularizer, preventing the potential distribution shifts.

Methods	Cora	Citeseer	PubMed	Computer	Photo	Co-CS	Co-Phys	Wiki-CS	Flickr	Arxiv
SIMMLP	**84.60**±0.24	**73.52**±0.53	**86.99**±0.09	**88.46**±0.16	**94.28**±0.08	**94.87**±0.07	**96.17**±0.03	**81.21**±0.13	**49.85**±0.09	**71.12**±0.10
w/o Rec.	84.37±0.27	73.18±0.24	86.86±0.10	88.25±0.07	94.15±0.07	94.64±0.06	96.01±0.07	81.10±0.13	49.60±0.11	70.38±0.22

F. Full Inductive Setting Results

Table 15 presents the comprehensive experimental results of the inductive (production) setting. We report the performance on both transductive and inductive sets, along with the interpolated production results. Note that the results of GLNN (Zhang et al., 2022) and NOSMOG (Tian et al., 2023) reported in this paper differ from their respective original papers. This is because our setting is more challenging where the inductive set is disconnected from the transductive set in inference. In this table, we present the performance of six baseline methods, which encompass supervised GNNs, self-supervised approaches, and MLP-based techniques. We can observe that our SIMMLP attains state-of-the-art performance in the majority of settings. Among GNN methods, we note that SAGE generally outperforms BGRL in transductive set, but underperforms it in inductive set. The robustness of BGRL stems from the augmentation, which aids in learning augmentation-invariant embeddings, enabling BGRL to work on inductive sets, even though the distributions of these two sets are potentially different. Regarding MLP-based methods, we observe that NOSMOG outperforms GLNN in transductive set, particularly on large-scale graphs, while GLNN significantly outperforms NOSMOG in inductive set. We assume that the distribution of positional embeddings of NOSMOG on the inductive set differs from the transductive set, rendering them untrustworthy and less meaningful. For our SIMMLP, the model maximizes the consistency between MLPs and GNNs in the embedding space, thereby preserving fine-grained and generalizable knowledge. This enables our model achieves the best performance.

Table 15. Node classification accuracy (%) under inductive (production) scenario for both transductive and inductive settings. *ind* represents the accuracy on $\mathcal{V}^I$, *trans* represents the accuracy on $\mathcal{V}_{test}^T$, and *prod* is the interpolated accuracy of both *ind* and *trans*.

	Setting	Cora	Citeseer	PubMed	Computer	Photo	Co-CS	Co-Phys	Wiki-CS	Flickr	Arxiv
SAGE	*prod*	77.51±1.77	68.40±1.61	85.04±0.44	87.24±0.43	93.20±0.45	92.88±0.40	95.74±0.12	**79.26±0.65**	47.17±0.73	68.52±0.56
	trans	79.46±1.49	68.73±1.37	85.57±0.30	87.98±0.30	93.70±0.42	93.13±0.33	95.77±0.04	80.01±0.41	48.15±0.63	**71.79±0.50**
	ind	69.70±2.89	67.11±2.57	82.90±0.98	84.45±0.94	91.18±0.56	91.87±0.68	95.63±0.05	76.27±1.63	43.25±1.14	55.45±0.78
BGRL	*prod*	77.73±1.07	64.33±1.56	83.97±0.48	87.33±0.48	91.47±0.62	91.26±0.35	94.38±0.29	76.25±1.09	49.12±0.31	69.29±0.38
	trans	77.32±0.90	64.15±1.40	83.97±0.34	87.27±0.42	91.47±0.51	91.31±0.33	94.40±0.25	76.32±0.97	49.09±0.24	70.36±0.35
	ind	79.38±1.74	65.03±2.19	83.98±1.02	**87.59±0.75**	91.46±1.05	91.09±0.45	94.33±0.46	75.96±1.57	49.26±0.60	65.03±0.50
MLP	*prod*	63.76±1.65	63.98±1.22	80.91±0.45	81.00±0.54	87.73±0.88	91.68±0.59	95.18±0.13	75.08±0.71	46.14±0.22	55.89±0.51
	trans	63.66±1.53	63.86±1.09	80.92±0.38	81.05±0.45	87.69±0.86	91.66±0.54	95.18±0.12	75.12±0.43	46.16±0.15	55.89±0.46
	ind	64.15±2.11	64.43±1.76	80.90±0.72	80.80±0.91	87.88±0.96	91.78±0.81	95.16±0.18	74.94±1.81	46.09±0.50	55.91±0.69
GLNN	*prod*	78.34±1.04	69.61±1.13	85.44±0.48	87.04±0.50	93.28±0.43	93.72±0.35	95.76±0.09	78.39±0.54	46.11±0.27	63.53±0.48
	trans	79.93±0.87	69.73±0.77	85.70±0.38	87.80±0.45	93.84±0.42	93.82±0.32	95.78±0.04	78.58±0.32	46.13±0.22	64.27±0.46
	ind	71.96±1.68	69.14±2.58	84.42±0.87	83.98±0.70	91.05±0.49	93.34±0.47	95.70±0.09	77.64±1.42	46.05±0.43	60.55±0.55
GENN	*prod*	77.83±1.57	67.30±1.48	84.34±0.47	85.75±1.20	92.09±0.96	93.57±0.37	95.67±0.06	78.27±1.01	45.56±0.51	68.52±0.54
	trans	80.27±1.41	67.86±1.16	85.81±0.38	87.42±1.04	93.35±0.60	93.79±0.35	95.78±0.05	80.31±0.85	45.68±0.45	70.01±0.50
	ind	68.09±2.21	65.07±2.78	78.44±0.84	79.09±1.84	87.05±2.42	92.68±0.45	95.23±0.08	70.13±1.65	45.08±0.74	62.58±0.69
NOSMOG	*prod*	77.83±1.94	68.58±1.41	83.84±0.45	86.61±1.22	92.52±0.68	93.45±0.44	95.78±0.10	78.35±0.70	46.05±0.55	69.10±0.80
	trans	80.27±1.69	68.95±1.24	85.43±0.37	**88.30±1.14**	**93.88±0.47**	93.68±0.38	95.85±0.10	**80.35±0.58**	46.24±0.51	70.50±0.79
	ind	68.11±2.95	67.07±2.10	77.44±0.80	79.83±1.52	87.08±1.52	92.55±0.69	95.52±0.10	70.36±1.18	45.27±0.72	63.49±0.83
SIMMLP	*prod*	**81.37±1.20**	**72.33±0.90**	**86.47±0.28**	**87.65±0.40**	**93.87±0.32**	**94.63±0.16**	**96.04±0.12**	**79.26±0.83**	**49.27±0.18**	**70.23±0.47**
	trans	**81.60±0.96**	**72.21±0.73**	**86.48±0.23**	87.67±0.25	93.86±0.26	**94.66±0.16**	**96.06±0.09**	79.46±0.66	**49.23±0.11**	71.25±0.33
	ind	**80.48±2.15**	**72.81±1.61**	**86.44±0.51**	87.58±0.99	**93.91±0.58**	**94.51±0.15**	**95.97±0.24**	**78.46±1.48**	**49.41±0.46**	**66.13±1.05**

G. Extension to Graph Classification

G.1. Datasets

All graph classification datasets are sourced from TU datasets (Morris et al., 2020)[4], including biochemical molecule datasets (**PTC-MR, MUTAG, DD, PROTEINS**) and social networks (**IMDB-B, IMDB-M, COLLAB**). Table 16 shows the statistics of these datasets. In PTC-MR and DD, we utilize the original node features, whereas for other datasets lacking rich node features, we generate one-hot features based on node degrees. We follow 10-fold cross-validation to evaluate model performance.

Table 16. The statistics of graph classification datasets.

Dataset	Task	# Graphs	# Nodes	# Edges	# Features	# Classes	Split
IMDB-B	Graph-level	1,000	∼19.8	∼193.1	-	2	10-fold CV
IMDB-M	Graph-level	1,500	∼13.0	∼65.9	-	3	10-fold CV
COLLAB	Graph-level	5,000	∼74.5	∼4,914.4	-	3	10-fold CV
PTC-MR	Graph-level	344	∼14.3	∼14.7	18	2	10-fold CV
MUTAG	Graph-level	118	∼17.9	∼39.6	7	2	10-fold CV
DD	Graph-level	1,178	∼284.3	∼715.6	89	2	10-fold CV
PROTEINS	Graph-level	1,113	∼39.1	∼145.6	3	2	10-fold CV

G.2. Baselines

Supervised GNNs. We utilize 5-layer **GIN** (Xu et al., 2019) as the baseline.

Self-supervised GNNs. For graph-level tasks, we explore traditional graph kernels for classification, including **WL kernel** (Shervashidze et al., 2011) and **DGK** (Yanardag & Vishwanathan, 2015). Furthermore, we include advanced contrastive learning approaches, such as **graph2vec** (Narayanan et al., 2017), **MVGRL** (Hassani & Khasahmadi, 2020), **InfoGraph** (Sun et al., 2020), **GraphCL** (You et al., 2020), and **JOAO** (You et al., 2021), which conduct contrastive learning between embeddings of two augmented graphs.

MLPs on Graphs. For standard **MLP**, we append a pooling function following the encoder to generate graph embeddings, which are utilized to perform predictions. Considering other MLP learning baselines, they cannot be directly applied on graph-level tasks. To this end, we extend GLNN (Zhang et al., 2022) to graph classification by distilling knowledge from pre-trained GINs to MLPs on graph-level embeddings, dubbed as **MLP + KD**.

Table 17. Hyper-parameters of SIMMLP on graph-level task.

Hyper-parameters	Graph Classification						
	IMDB-B	IMDB-M	COLLAB	PTC-MR	MUTAG	DD	PROTEINS
Epochs	200	100	30	100	100	100	500
Optimizer	AdamW used for all datasets						
Learning Rate	1e-2	1e-2	5e-4	1e-2	1e-2	1e-3	1e-3
Weight Decay	0 used for all datasets						
Activation	PReLU used for all datasets						
Batch Size	64	128	32	64	64	32	64
Raw Feature	N	N	N	Y	N	Y	N
Deg4Feature	Y	Y	Y	N	Y	N	Y
Pooling	MEAN	MEAN	MEAN	SUM	SUM	MEAN	SUM
Hidden Dimension	512 used for all datasets						
Normalization	Batchnorm used for all datasets						
# Encoder Layers	2 used for all datasets						
# Aggregator Layers	2	2	2	2	1	2	1
Feature Mask Ratio	0.50	0.25	0.75	0.25	0.5	0.00	0.00
Edge Mask Ratio	0.75	0.50	0.75	0.00	0.25	0.00	0.50

[4]These datasets are available in PyG library.

G.3. Experimental Settings

The experimental setting is the same as Sec. B.3. The only exclusion is we utilize a 5-layer GIN (Xu et al., 2019) as the encoder. The readout function are selected from {MEAN, SUM, MAX}. The hyper-parameters of SIMMLP is in Table 17.

G.4. Results

Table 18. The performance on graph classification tasks with accuracy (%).

	Methods	IMDB-B	IMDB-M	COLLAB	PTC-MR	MUTAG	DD	PROTEINS
Supervised	GIN (Xu et al., 2019)	75.10±5.10	52.30±2.80	80.20±1.90	64.60±1.70	89.40±5.60	74.88±3.12	76.20±2.80
Graph Kernel	WL (Shervashidze et al., 2011)	72.30±3.44	46.95±0.46	-	57.97±0.49	80.72±3.00	-	72.92±0.56
	DGK (Yanardag & Vishwanathan, 2015)	66.96±0.56	44.55±0.52	-	60.08±2.55	87.44±2.72	-	73.30±0.82
GCL	graph2vec (Narayanan et al., 2017)	71.10±0.54	50.44±0.87	-	60.17±6.86	83.15±9.25	-	73.30±2.05
	MVGRL (Hassani & Khasahmadi, 2020)	71.84±0.78	50.84±0.92	73.10±0.56	-	**89.24±1.31**	75.20±0.55	74.02±0.32
	InfoGraph (Sun et al., 2020)	73.03±0.87	49.69±0.53	70.65±1.13	**61.65±1.43**	89.01±1.13	72.85±1.78	74.44±0.31
	GraphCL (You et al., 2020)	71.14±0.44	48.58±0.67	71.36±1.15	-	86.80±1.34	**78.62±0.40**	74.39±0.45
	JOAO (You et al., 2021)	70.21±3.08	49.20±0.77	69.50±0.36	-	87.35±1.02	-	74.55±0.41
MLP	MLP*	49.50±1.66	33.11±1.59	51.90±0.95	54.39±1.41	67.22±0.99	58.56±1.40	59.20±1.00
	MLP + KD*	72.85±1.04	48.14±0.52	75.38±1.53	59.38±1.38	87.44±0.67	73.59±1.69	73.54±1.78
	SIMMLP (Ours)	**74.06±0.22**	**51.41±0.52**	**81.04±0.11**	60.28±1.07	87.67±0.24	78.44±0.47	**75.31±0.13**

The reported results of baselines are from previous papers if available (You et al., 2020; 2021; Hou et al., 2022). * indicates the results are from our implementation.

In this section, we present the experimental results of SIMMLP alongside state-of-the-art graph classification baselines, shown in Table 18. Compared to existing MLP learning methods, SIMMLP enjoys the benefit inherent in self-supervised learning, which enables SIMMLP to be readily extended into multiple downstream tasks (Sun et al., 2023). We observe that SIMMLP achieves the best or sub-best performance on 6 out of 7 datasets, especially on the large-scaled COLLAB, highlighting the potential of MLP-based methods in graph-level tasks. However, other MLP-based methods underperform self-supervised GCL baselines and even traditional graph kernel methods. This might because the graph-level knowledge is hard to encode when only leveraging node features. Overall, SIMMLP expands the application of MLPs from node-level tasks to graph-level tasks.

H. Extension to Supervised SIMMLP

SIMMLP follows the self-supervised learning paradigm where the encoder and prediction head are trained separately. Despite the benefit on generalization (Huang et al., 2023) and robustness (Hendrycks et al., 2019), the performance of self-supervised learning methods typically lags behind its supervised counterparts (Chen et al., 2020b). To analyze this on our method, we implement a supervised SIMMLP by jointly optimizing the alignment loss in Equation 4 and downstream task loss:

$$\mathcal{L} = \sum_{i\in\mathcal{V}} \|\rho(\boldsymbol{h}_i^{MLP}) - \boldsymbol{h}_i^{GNN}\|^{2\gamma} + \lambda \sum_{i\in\mathcal{V}} \|\mathcal{D}(\boldsymbol{h}_i^{GNN}) - \boldsymbol{x}_i\|^2 + \beta \sum_{j\in\mathcal{V}_{train}} \mathcal{L}_{CE}(\hat{\boldsymbol{y}}_j^{MLP}, \boldsymbol{y}_j). \tag{30}$$

For simplicity, we search the value of β within $\{0.1, 1, 10\}$, and conduct experiments on transductive node classification, while the model can be readily extended to inductive and cold-start settings. Beyond our expectation, the self-supervised version can outperform the supervised counterpart on 7 out of 10 datasets, shown in Table 19. We assume the counterintuitive observation derives from the noise imposed by cross-entropy loss on model optimization. Particularly, optimizing the cross-entropy loss would introduce additional gradients on model parameters, which can affect the direction and length of model optimization. This additional gradients may lead the model to learn pseudo-correlations between GNNs and MLPs, thus impairing the alignment process.

Table 19. Ablation study on the model with or without supervision.

	Cora	Citeseer	PubMed	Computer	Photo	Co-CS	Co-Phys	Wiki-CS	Flickr	Arxiv
`sup.`	77.23±1.41	**75.20±0.55**	**88.64±0.27**	**88.68±0.25**	94.17±0.18	94.60±0.19	95.89±0.10	80.64±0.34	46.39±1.73	70.60±0.43
`w/o sup.`	**84.60±0.24**	73.52±0.53	86.99±0.09	88.46±0.16	**94.28±0.08**	**94.87±0.07**	**96.17±0.03**	**81.21±0.13**	**49.85±0.09**	**71.12±0.10**